Structured Sparse Coding-Based Hyperspectral Imagery Denoising With Intracluster Filtering

Wei Wei, *Member, IEEE*, Lei Zhang, *Student Member, IEEE*, Chunna Tian, *Member, IEEE*, Antonio Plaza, *Fellow, IEEE*, and Yanning Zhang, *Senior Member, IEEE*

***Abstract*— Sparse coding can exploit the intrinsic sparsity of hyperspectral images (HSIs) by representing it as a group of sparse codes. This strategy has been shown to be effective for HSI denoising. However, how to effectively exploit the structural information within the sparse codes (structured sparsity) has not been widely studied. In this paper, we propose a new method for HSI denoising, which uses structured sparse coding and intracluster filtering. First, due to the high spectral correlation, the HSI is represented as a group of sparse codes by projecting each spectral signature onto a given dictionary. Then, we cast the structured sparse coding into a covariance matrix estimation problem. A latent variable-based Bayesian framework is adopted to learn the covariance matrix, the sparse codes, and the noise level simultaneously from noisy observations. Although the considered strategy is able to perform denoising through accurately reconstructing spectral signatures, an inconsistent recovery of sparse codes may corrupt the spectral similarity in each spatial homogeneous cluster within the scene. To address this issue, an intracluster filtering scheme is further employed to restore the spectral similarity in each spatial cluster, which results in better denoising results. Our experimental results, conducted using both simulated and real HSIs, demonstrate that the proposed method outperforms several state-of-the-art denoising methods.**

***Index Terms*— Covariance matrix estimation, hyperspectral images (HSIs) denoising, intracluster filtering, structured sparse coding.**

I. Introduction

HYPERSPECTRAL imaging is a technique that collects the spectral information across a certain range of the electromagnetic spectrum at narrow wavelengths (e.g., 10 nm) [1]. The obtained hyperspectral images (HSIs) thus exhibit an approximately continuous spectrum at each pixel. Such wealth of spectral information enables HSIs to better represent the imaged scene and thus greatly enhance the performance of extensive practical applications, such as target detection [2], [3], scene classification [4], [5], and video tracking [6]. However, HSIs are often affected by noise during image collection, transmission, etc. [7], [8], and the noise level varies across bands [9], [10]. Since the performance of many applications (e.g., classification [11]) is sensitive to noise, HSIs denoising is one of the fundamental steps prior to HSI exploitation. According to the relation to signal, noise on HSIs can be roughly divided into two types, namely, signal-dependent noise and signal-independent noise. Both types have been widely studied in HSIs denoising [8]. In this paper, we mainly focus on methods for signal-independent noise.

To date, many effective HSI denoising methods have been proposed. For example, by considering the HSI as a third tensor, the low-rank tensor approximation (LRTA) was employed in [12] for denoising purposes. Liu *et al.* [13] exploited the parallel factor (PARAFAC) analysis model to decompose the HSI tensor as a sum of several rank-1 tensors. The noise was expected to be reduced by exploring the low-rank characteristics of the HSIs. As opposed to these methods that consider the whole HSI in the denoising process, Peng *et al.* [8] collected similar full band patches to form a cluster tensor. Then, a group-block-sparsity constraint was imposed on the cluster tensor to restrict the nonlocal spectrum similarity in a tensor decomposition framework, which led to better denoising performance. In addition to these tensor-based methods, some existing 2-D image denoising methods have been extended for HSIs. Based on the nonlocal means (NLM) filter [14] method, Qian *et al.* [15] extended the spatially local patches to a spatial–spectral local tensor in order to explore the spectral–spatial correlation in HSIs. Block-matching and 3-D filtering [16], which groups the similar 2-D patches together to enhance the sparsity and employs collaborative filtering, has achieved state-of-the-art denoising performance on traditional images. Inspired by this, Maggioni *et al.* [17] proposed a block-matching and 4-D (BM4D) filtering method for HSIs.

In recent years, sparse coding (which exploits the intrinsic sparsity of HSIs by representing them as a group of sparse codes on a proper dictionary) has demonstrated effectiveness. For example, Dabov *et al.* [16] employed ℓ_1 norm to model the intrinsic sparsity of HSIs on an overcomplete 3-D wavelet dictionary. In [18], ℓ_1 norm-based sparsity regularization

Manuscript received August 11, 2016; revised May 10, 2017; accepted July 19, 2017. Date of publication August 22, 2017; date of current version November 22, 2017. This work was supported in part by the National Natural Science Foundation of China under Grant 61671385, Grant 61231016, Grant 61571354, and Grant 61301192, in part by the Natural Science Basis Research Plan in Shaanxi Province of China under Grant 2017JM6021 and Grant 2017JM6001, in part by the China Postdoctoral Science Foundation under Grant 158201, and in part by the Innovation Foundation for Doctoral Dissertation of Northwestern Polytechnical University under Grant CX201521. *(Wei Wei and Lei Zhang contributed equally to this work.) (Corresponding author: Lei Zhang.)*

W. Wei, L. Zhang, and Y. Zhang are with the Shaanxi Provincial Key Laboratory of Speech and Image Information Processing, School of Computer Science and Engineering, Northwestern Polytechnical University, Xi'an 710072, China (e-mail: weiweinwpu@nwpu.edu.cn; zhanglei211@mail.nwpu.edu.cn; ynzhang@nwpu.edu.cn).

C. Tian is with the School of Electronic Engineering, Xidian University, Xi'an 710071, China (e-mail: chnatian@xidian.edu.cn).

A. Plaza is with the Hyperspectral Computing Laboratory, Department of Technology of Computers and Communications, Escuela Politécnica, University of Extremadura, 10071 Cáceres, Spain (e-mail: aplaza@unex.es).

Color versions of one or more of the figures in this paper are available online at http://ieeexplore.ieee.org.

Digital Object Identifier 10.1109/TGRS.2017.2735488

was used to reconstruct the HSI with an singular value decomposition and wavelets-based image model. Recently, it has been found that some meaningful structures exist within the sparse code [19], e.g., the tree structure in the wavelet transformation coefficients [20], [21], clustered structure in musical signals [22], or the block structure [23]. Huang *et al.* [24] theoretically proved that exploring those meaningful structures (termed structured sparse coding) improved the reconstruction accuracy of standard sparse coding. Structured sparse coding has already shown effectiveness in some practical applications, e.g., compressive sensing [25], [26] and denoising [10]. However, the structured sparse coding is rarely exploited for HSIs denoising, namely, how to exploit the structured sparsity to enhance the performance of HSI denoising is still an open problem.

In this paper, we propose a novel HSI denoising method that combines structured sparse coding and intracluster filtering to improve denoising performance. Specifically, since each pixel in the HSI contains an approximately continuous spectrum, we sparsely represent each spectrum on a given spectrum dictionary. In other words, we obtain a sparse code for each spectrum. Through modeling all obtained sparse codes together with a full covariance matrix-based normal distribution, we simplify the structured sparse coding into a covariance matrix estimation problem. We employ a latent variable-based Bayesian framework to explore the data-dependent structured sparsity within each spectrum, where the covariance matrix, sparse codes, and noise level are simultaneously learned from the noisy observations. This approach is able to improve the reconstruction accuracy of spectra. However, an inconsistent recovery of sparse codes may be obtained when modeling those sparse codes independently. This may corrupt the spectral similarity in spatially homogeneous clusters in the scene, thus limiting the performance of structured sparse coding for HSI denoising. To address this issue, an intracluster filtering scheme is further employed to restore the spectral similarity in each spatial cluster. To demonstrate the effectiveness of our newly proposed method, we compare it with several state-of-the-art methods using both simulated and real noisy HSIs.

The remainder of this paper is structured as follows. Section II gives a brief introduction on sparse coding of HSIs. The proposed method is illustrated in Section III. The optimization procedure is given in Section IV. Experimental results and analysis are provided in Section V, and Section VI concludes this paper with some remarks.

II. Background of Sparse Coding

Let us consider a 3-D HSI $\mathcal{X} \in \mathbb{R}^{n_r \times n_c \times n_b}$ that contains n_r rows and n_c columns. Each pixel is an n_b-D vector. In this paper, we represent the HSI as a 2-D matrix $X \in \mathbb{R}^{n_b \times n_p}$, where each row stacks a vectorized 2-D spatial band image with $n_p = n_r \times n_c$ pixels, and each column denotes one spectrum. Since the 2-D spatial domain and the continuous spectrum domain are both highly correlated (i.e., 3-D redundancy), the HSI can be sparsely represented on a spectrum dictionary [26], [27], a spatial path dictionary [28], or even a 3-D dictionary [16], [17]. In this paper, we mainly focus on sparsifying the HSI with a proper spectrum dictionary to explore the sparsity within each spectrum. Given a proper spectrum dictionary $D \in \mathbb{R}^{n_b \times n_d}$, each spectrum can be represented by a sparse code. The corresponding sparse coding of X can be formulated as follows:

$$\min_{Y} \sum_{i=1}^{n_p} \|\boldsymbol{y}_i\|_0, \quad \text{s.t.} X = DY \tag{1}$$

where $Y = [\boldsymbol{y}_1, \ldots, \boldsymbol{y}_{n_p}] \in \mathbb{R}^{n_d \times n_p}$ denotes all sparse codes and the column vector $\boldsymbol{y}_i$ indicates the sparse code for the spectrum associated with the ith pixel. $\|\boldsymbol{y}_i\|_0$ denotes the ℓ_0 norm of $\boldsymbol{y}_i$, which counts the nonzero components in $\boldsymbol{y}_i$. When considering the representation error, the sparse coding can be reformulated as

$$\min_{Y} \sum_{i=1}^{n_p} \|\boldsymbol{y}_i\|_0, \quad \text{s.t.} \|X - DY\|_F^2 \leq \epsilon \tag{2}$$

where ϵ is a predefined scalar determined by the representation error and $\|\cdot\|_F$ indicates the Frobenius norm. Due to the ℓ_0 norm, it is NP hard to solve (1) or (2). Thus, when some mild conditions are satisfied, ℓ_0 norm is often substituted by the ℓ_p norm with $0 < p \leq 1$, which casts the sparse coding into a convex or nonconvex optimization problem as

$$\min_{Y} \sum_{i=1}^{n_p} \|\boldsymbol{y}_i\|_p, \quad \text{s.t.} \|X - DY\|_F^2 \leq \epsilon \tag{3}$$

where $\|\boldsymbol{y}_i\|_p = (\sum_{j=1}^{n_d} |y_{ji}|^p)^{1/p}$ and y_{ji} is the jth component in $\boldsymbol{y}_i$. For example, when the restricted isometry property holds, ℓ_0 norm can be equally replaced by ℓ_1 norm, which results in a convex optimization problem. Most sparse coding-based HSI denoising methods directly utilize (2), (3), or their variants. Since the noise-free HSI can be sparsely represented on a proper dictionary while noise cannot, sparse coding has exhibited good performance for HSIs denoising. However, sparse coding models each component in the sparse code independently. For example, ℓ_1 norm on $\boldsymbol{y}_i$ equals the following prior distribution:

$$\begin{aligned} p(\boldsymbol{y}_i) \propto \exp(-\alpha \|\boldsymbol{y}_i\|_1) &= \exp\left(-\sum_{j=1}^{n_d} \alpha |y_{ji}|\right) \\ &= \prod_{j=1}^{n_d} \exp(-\alpha |y_{ji}|) \end{aligned} \tag{4}$$

where α is a predefined scalar. From (4), we can find that ℓ_1 norm on $\boldsymbol{y}_i$ amounts to imposing the identity independent distribution on each component y_{ji}. Thus, they fail to capture the underlying structure within the sparse code.

To address this problem, structured sparse coding has been adopted in recent years, which has proved to perform better in representation than the standard sparse coding shown in (2) or (3) [24]. Therefore, it is natural to harness the structured sparse coding to enhance the denoising performance of HSIs. To this end, we will engineer a novel structured sparse coding model of HSIs in the Bayesian way in this paper.

III. Proposed Method

In this paper, we mainly focus on the additive noise corruption on HSIs, and thus the noisy observation model can be formulated as

$$F = X + N = DY + N \tag{5}$$

where $F \in \mathbb{R}^{n_b \times n_p}$ denotes the noisy observation and $N \in \mathbb{R}^{n_b \times n_p}$ indicates the random noise. According to Section II, X can be sparsely represented on a given spectrum dictionary D as $X = DY$. Each column of Y denotes a sparse code. Considering that the noise level varies across bands [9], we assume that X is corrupted by various levels of Gaussian white noise across bands. Thus, N can be modeled by a matrix normal distribution as $\mathcal{MN}(0, \Sigma_n, I)$, where $\Sigma_n = \mathbf{diag}(\boldsymbol{\lambda})$[1] represents the noise variances across bands with $\boldsymbol{\lambda} = [\lambda_1, \ldots, \lambda_{n_b}]^T$. I is an identity matrix with proper size and implies that noise corruption in each column of X is independent. By defining a weighted trace norm operation $\|Q\|_{\Sigma_n} = (\mathbf{tr}(Q^T \Sigma_n^{-1} Q))^{1/2}$, we can formulate the likelihood of the noisy observation as

$$p(F|Y, \boldsymbol{\lambda}) \propto |\Sigma_n|^{-n_p/2} \exp\left\{-\frac{1}{2}\|DY - F\|^2_{\Sigma_n}\right\}. \tag{6}$$

A. Structured Sparsity Prior

A zero-mean matrix normal distribution is utilized to model Y as

$$\begin{aligned} p(Y|\Sigma_y) &\propto |\Sigma_y|^{-n_p/2} \exp\left\{-\frac{1}{2}\|Y\|^2_{\Sigma_y}\right\} \\ &= \prod_{i=1}^{n_p} |\Sigma_y|^{-1/2} \exp\left(-\frac{1}{2}\boldsymbol{y}_i^T \Sigma_y^{-1} \boldsymbol{y}_i\right) \end{aligned} \tag{7}$$

where $\Sigma_y \in \mathbb{R}^{n_d \times n_d}$ is the covariance matrix indicating the correlation among different rows of Y. In previous Bayesian sparse learning schemes [29], [30], Σ_y is assumed to be diagonal. When a diagonal component $\Sigma_y(j, j)$ approaches zero, the jth dimension y_{ji} of the sparse code $\boldsymbol{y}_i$ also tends to be zero and vice versa. Therefore, a plausible diagonal Σ_y can depict the sparsity of the considered signal. However, when Σ_y is diagonal, (7) fails to capture the structure within the sparse code, because (7) in this case amounts to imposing independent priors on each component of the sparse code $\boldsymbol{y}_i$ as follows:

$$\begin{aligned} p(\boldsymbol{y}_i|\Sigma_y) &\propto |\Sigma_y|^{-1/2} \exp\left(\boldsymbol{y}_i^T \Sigma_y^{-1} \boldsymbol{y}_i\right) \\ &= \prod_{j=1}^{n_d} [\Sigma_y(j, j)]^{-1/2} \exp\left[-y_{ji}^2/(2\Sigma_y(j, j))\right]. \end{aligned} \tag{8}$$

To capture the underlying structure within each sparse code, we adopt a full covariance matrix Σ_y for (7). In the following, we will illustrate our motivation using a probabilistic graph model theory. Provided that the sparse code $\boldsymbol{y}_i$ lies in an undirected graph and each component y_{ji} denotes a node in the graph, the probability distribution of $\boldsymbol{y}_i$ can be modeled using Markov random field (MRF) as

$$p(\boldsymbol{y}_i) = \frac{1}{Z} \exp\left\{-\sum_j \phi(y_{ji}) - \sum_{j,k\neq j} \psi(y_{ji}, y_{ki})\right\} \tag{9}$$

where we only consider the unary potential $\phi(y_{ji})$ and the pairwise potential $\psi(y_{ji}, y_{ki})$. Z is the normalization term. Since the correlation among different nodes can be well represented by the pairwise correlation, this MRF model is able to represent the underlying graph structure within $\boldsymbol{y}_i$. When $\phi(y_{ji}) = \Sigma_y^{-1}(j, j) y_{ji}$ and $\psi(y_{ji}, y_{ki}) = \Sigma_y^{-1}(j, k) y_{ji} y_{ki}$ are both linear functions, $p(\boldsymbol{y}_i|\Sigma_y)$ can be reformulated as

$$\begin{aligned} p(\boldsymbol{y}_i) &= \frac{1}{Z} \exp\left\{-\sum_{jk} \Sigma_y^{-1}(j, k) y_{ji} y_{ki}\right\} \\ &\propto |\Sigma_y|^{-1/2} \exp\left(-\frac{1}{2}\boldsymbol{y}_i^T \Sigma_y^{-1} \boldsymbol{y}_i\right). \end{aligned} \tag{10}$$

This means that the prior in (7) with a full covariance matrix Σ_y depicts an undirected graph structure within each $\boldsymbol{y}_i$. Specifically, the components in Σ_y^{-1} denote the weights in the linear unary and pairwise potentials, and the corresponding pairwise potentials model the correlation among components in each $\boldsymbol{y}_i$. In addition, the sparsity of each $\boldsymbol{y}_i$ is represented by the unary term as traditional Bayesian sparse learning [29], [30]. Therefore, the prior in (7) with a full covariance matrix Σ_y can model the structured sparsity of Y more suitably, compared with a diagonal Σ_y.

To further clarify this point, we sparsify each spectrum from a real HSI [shown in Fig. 1(a)] on an orthogonal wavelet dictionary and the corresponding sparse codes Y of the first 200 pixels are shown in Fig. 1(b). It has shown that a tree structure exists within each obtained sparse code [20], [21]. To illustrate that those structured sparse codes exhibit a nondiagonal covariance matrix, we obtain the empirical covariance matrix [2] on all sparse codes, which represents the correlation among different components of each sparse code [shown in Fig. 1(c)]. It can be seen that the obtained covariance matrix is nondiagonal. Therefore, in the following, we will mainly focus on how to estimate a plausible covariance matrix Σ_y to represent the structured sparsity of Y.

B. Latent Variable-Based Structured Sparse Coding

To infer the clean image X from the noisy observation F with the structured sparsity prior in (7), we have to infer the graph structure (i.e., Σ_y) as a prior. Many previous works learned a general graph structure from extensive training examples [31]–[33]. However, the learned general structure cannot well fit the specific data distribution and thus leads to limited denoising performance. In this paper, we instead try to learn the data-dependent graph structure directly from the noisy observations. To this end, we first introduce a hyperprior on the covariance matrix Σ_y for learning more flexible graph structure. There are mainly two kinds of priors. When there is some known prior information

[1] $\mathbf{diag}(\cdot)$ denotes the 'diag()' function in MATLAB.

[2] The covariance matrix is obtained as cov(Y') in MATLAB.

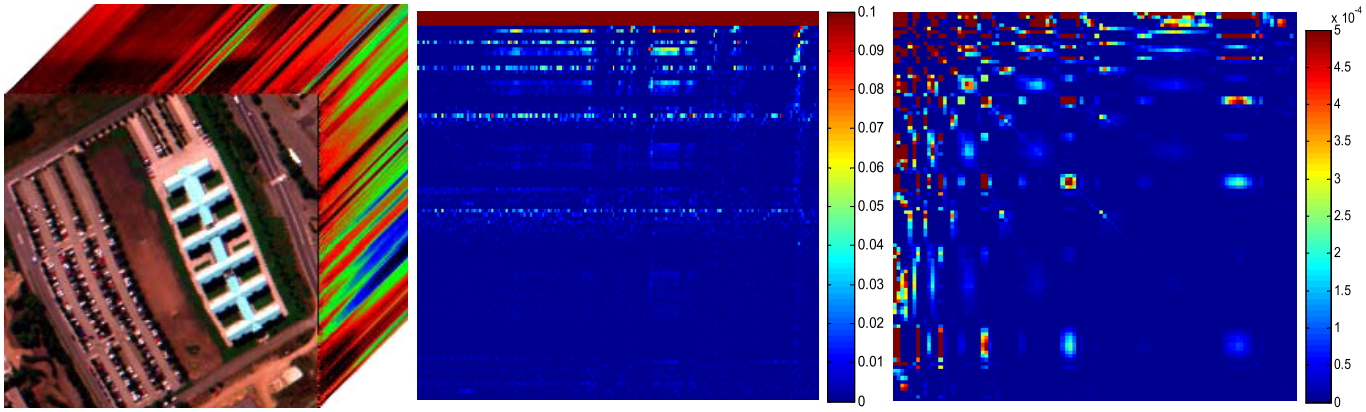

(a) (b) (c)

Fig. 1. Structured sparse codes of the spectra in a real HSI on an orthogonal wavelet dictionary. (a) 3-D data cubes. (b) Sparse codes of the spectra on the first 200 pixels in the HSI, where each column denotes a sparse code. (c) Nondiagonal covariance matrix of the sparse codes, which represents the correlation among different components within each sparse code. It can be seen that the structured sparsity within each code results in a nondiagonal covariance matrix.

of Σ_y (e.g., specific structure [34]), we can impose an inverse-Wishart distribution on Σ_y as

$$p(\Sigma_y) \propto |\Sigma_y|^{(n_p+l+1)/2} \exp\left[-\frac{1}{2}\mathbf{tr}\left(\Theta\,\Sigma_y^{-1}\right)\right] \tag{11}$$

where Θ is a reference matrix with prior information of Σ_y and l denotes the degree of freedom. This prior encourages Σ_y to approach the reference matrix Θ. However, only some special applications (see [34]) have available prior information. In most cases, there is no prior information on Σ_y. To handle the cases without any prior information, we impose the noninformative prior on each component of Σ_y as

$$p(\Sigma_y(i,j)) \propto \frac{1}{t} \tag{12}$$

where t is a given scalar. This prior encourages to learn the Σ_y directly from the observed data without any prior information. Since we expect to adapt the imposed structured sparsity prior to the data distribution, we adopt the second prior in this paper.

With this noninformative prior on Σ_y, we then employ a latent variable-based Bayesian framework to estimate Σ_y and noise level $\boldsymbol{\lambda}$ from the noisy observation F as

$$\max_{\Sigma_y,\boldsymbol{\lambda}} p(\Sigma_y,\boldsymbol{\lambda}|F) \propto \int p(F|Y,\boldsymbol{\lambda})p(Y|\Sigma_y)\prod_{ij} p(\Sigma_y(i,j))dY. \tag{13}$$

where Y acts as the latent variable. To clarify the relationship between variables, the hierarchical structure of this model is given in Fig. 2. By introducing the negative logarithm operation, (13) can be formulated as

$$\min_{\Sigma_y,\boldsymbol{\lambda}} \mathbf{tr}\left(F^T\Sigma_m^{-1}F\right) + n_p \log|\Sigma_m| \tag{14}$$

where $\Sigma_m = \Sigma_n + D\Sigma_y D^T$. If the optimal Σ_y and $\boldsymbol{\lambda}$ have been learned from (14), the sparse codes Y can be inferred by the maximum *a posteriori* (MAP) estimation based on the likelihood in (6) and structured sparsity prior in (7) as

$$\max_{Y} p(Y|F) \propto p(F|Y,\boldsymbol{\lambda})p(Y|\Sigma_y). \tag{15}$$

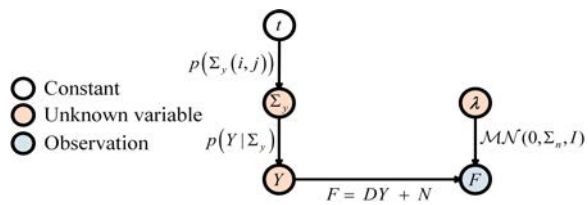

Fig. 2. Hierarchical structure of the proposed latent variable-based structured sparse coding.

However, it is intractable to solve (14) directly. Inspired by [26], we have the following relationship:

$$\mathbf{tr}\left(F^T\Sigma_m^{-1}F\right) = \min_{Y} \|DY - F\|^2_{\Sigma_n} + \|Y\|^2_{\Sigma_y} \tag{16}$$

which leads to a restrictive upper bound of $\mathbf{tr}(F^T\Sigma_m^{-1}F)$ as

$$\forall Y, \mathbf{tr}\left(F^T\Sigma_m^{-1}F\right) \le \|DY - F\|^2_{\Sigma_n} + \|Y\|^2_{\Sigma_y}. \tag{17}$$

Substituting this upper bound into (14), we obtain a unified optimization formula as

$$\min_{Y,\Sigma_y,\boldsymbol{\lambda}} \|DY - F\|^2_{\Sigma_n} + \|Y\|^2_{\Sigma_y} + n_p \log|\Sigma_m| \tag{18}$$

where the sparse codes Y, covariance matrix Σ_y, and noise level $\boldsymbol{\lambda}$ are jointly modeled. More importantly, (18) can be effectively solved as seen in Section IV. Inspired by [27] and [26], we can prove that the optimum Y from (18) equals to that from the MAP estimation in (15) with those learned Σ_y and $\boldsymbol{\lambda}$ from (14). Therefore, we need to solve only the unified optimization in (18) for structured sparse coding.

Since the sparse codes Y, covariance matrix Σ_y, and noise level $\boldsymbol{\lambda}$ can be jointly optimized from the noisy observation, the learned structure of Y is data dependent and robust to the unknown noise, which guarantees to reconstruct the sparse codes accurately. Given the learned sparse codes Y from (18), the denoised HSI can be obtained as $\hat{X} = DY$.

C. Intracluster Filtering

Although the proposed structured sparse coding can recover a clean HSI from its noisy observation, the inconsistent recovery of sparse codes caused by modeling them independently

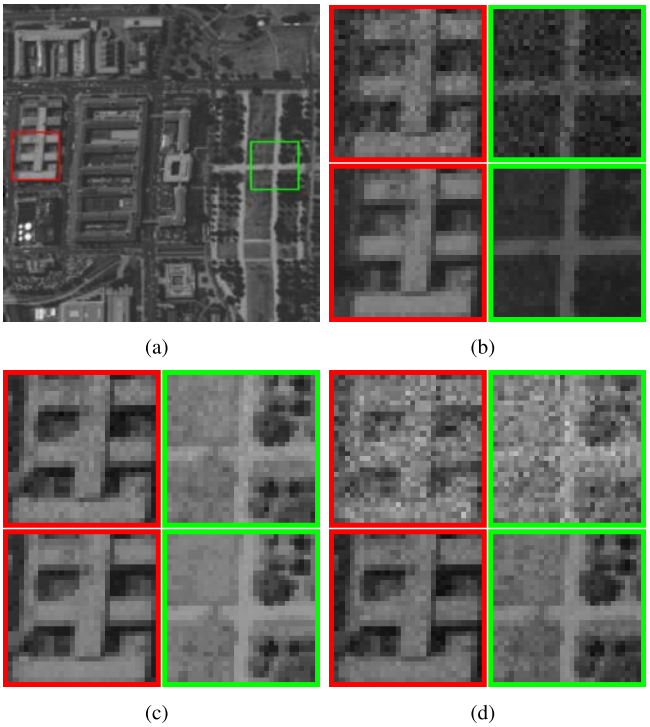

Fig. 3. Unnatural spatial appearance caused by the inconsistent recovery of sparse codes in structured sparse coding. (a) HSI data with two areas of interest marked by color windows. (b)–(d) Zoomed-in areas in the 20th, 63th, and 120th bands of the denoised results. (First row) The results from structured sparse coding alone. (Second row) The results from structured sparse coding together with intracluster filtering. It can be seen that the unnatural spatial appearance can be well restored by the proposed intraclustering filtering.

in (7) may limit the denoising performance. Specifically, natural scenes often exhibit spatially local and nonlocal similarity [8], [35]. Since homogeneous materials share similar spectral signatures [1], spatially local and nonlocal similarity of HSIs should be preserved. To jointly consider the local and nonlocal similarity in the spatial domain, we assume that a clean HSI can be spatially divided into K homogeneous clusters according to the spectral similarity. Thus, each cluster contains similar spectra from local and nonlocal similar pixels. This provides a strong prior for clean HSIs. However, the inconsistent recovery of sparse codes corrupts the spectral similarity in each spatial homogeneous cluster within the HSI, which may produce an unnatural spatial appearance, as illustrated in the first row of Fig. 3(b)–(d).

To restore the spectral similarity in each cluster, we develop an intracluster filtering method. Specifically, we employ a clustering method (e.g., K-means++ [36]) to spatially divide the HSI $\hat{X}$ reconstructed in Section III-B into K clusters based on the spectral similarity. Let $\hat{X}_k = [\hat{\boldsymbol{x}}_k^1, \ldots, \hat{\boldsymbol{x}}_k^{n_k}] \in \mathbb{R}^{n_b \times n_k}$ denote the spectra of pixels in the kth cluster, where n_k denotes the pixels number in this cluster. $\hat{\boldsymbol{x}}_k^i$ is the spectrum of the ith pixel in $\hat{X}_k$, which is filtered as

$$\bar{\boldsymbol{x}}_k^i = \sum_{j \neq i}^{n_k} w_{ij} \hat{\boldsymbol{x}}_k^j, \quad w_{ij} = \frac{1}{W_i} \exp\left(- \|\hat{\boldsymbol{x}}_k^i - \hat{\boldsymbol{x}}_k^j\|_2^2 / h \right) \quad (19)$$

where $\bar{\boldsymbol{x}}_k^i$ denotes the filtered spectrum of the ith pixel. $W_i = \sum_{j \neq i}^{n_k} w_{ji}$ is a normalization factor and h is a predetermined scalar. It can be seen that spectrum $\hat{\boldsymbol{x}}_k^j$ will be allocated a larger weight when it is more similar to $\hat{\boldsymbol{x}}_k^i$. With this filtering scheme, the unnatural spatial appearance produced by the structured sparse coding can be properly restored, as shown in the second row of Fig. 3(b)–(d). Moreover, the filtering scheme is able to remove the non-Gaussian noise (e.g., stripe noise) in real noisy HSIs, which will be illustrated in Section V-B. The proposed intracluster filtering scheme is different with regard to NLM [14], which employs the whole image to restore each pixel. In the proposed method, the spectrum of each pixel is restored only by the spectra of pixels in the same cluster, which results in an efficient algorithm.

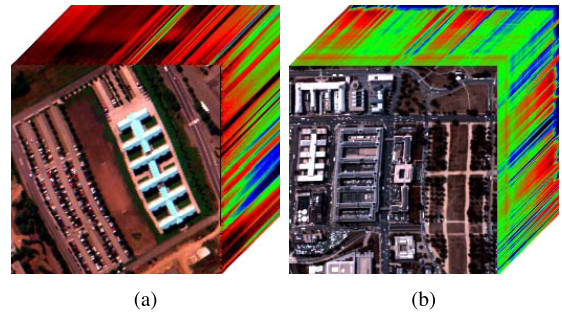

Fig. 4. 3-D cubes of (a) PaviaU and (b) Wdc with partial bands.

IV. Optimization and Full Procedure

In this section, we first describe the optimization for (18), and then provide the full procedure of our newly developed denoising algorithm. Since the optimization problem in (18) involves several unknown variables, it is difficult to optimize it directly. Inspired by [27] and [26], we utilize the alternative minimization scheme [27] to reduce the original problem in (18) to several subproblems, each of which involves only one unknown variable. We name these subproblems sparse coding, graph structure learning, and noise estimation. Then, those subproblems are alternatively optimized till convergence.

A. Sparse Coding: Optimization of Y

By removing those irrelevant terms, we obtain the subproblem of Y as

$$\min_{Y} \|DY - F\|_{\Sigma_n}^2 + \|Y\|_{\Sigma_y}^2. \quad (20)$$

Given Σ_y and $\boldsymbol{\lambda}$, this quadratic optimization problem has a closed-form solution as

$$Y = \Sigma_y D^T (\Sigma_n + D \Sigma_y D^T)^{-1} F. \quad (21)$$

B. Graph Structure Learning: Optimization of Σ_y

Given Y and $\boldsymbol{\lambda}$, the subproblem of Σ_y can be written as

$$\min_{\Sigma_y} \|Y\|_{\Sigma_y}^2 + n_p \log |\Sigma_n + D \Sigma_y D^T|. \quad (22)$$

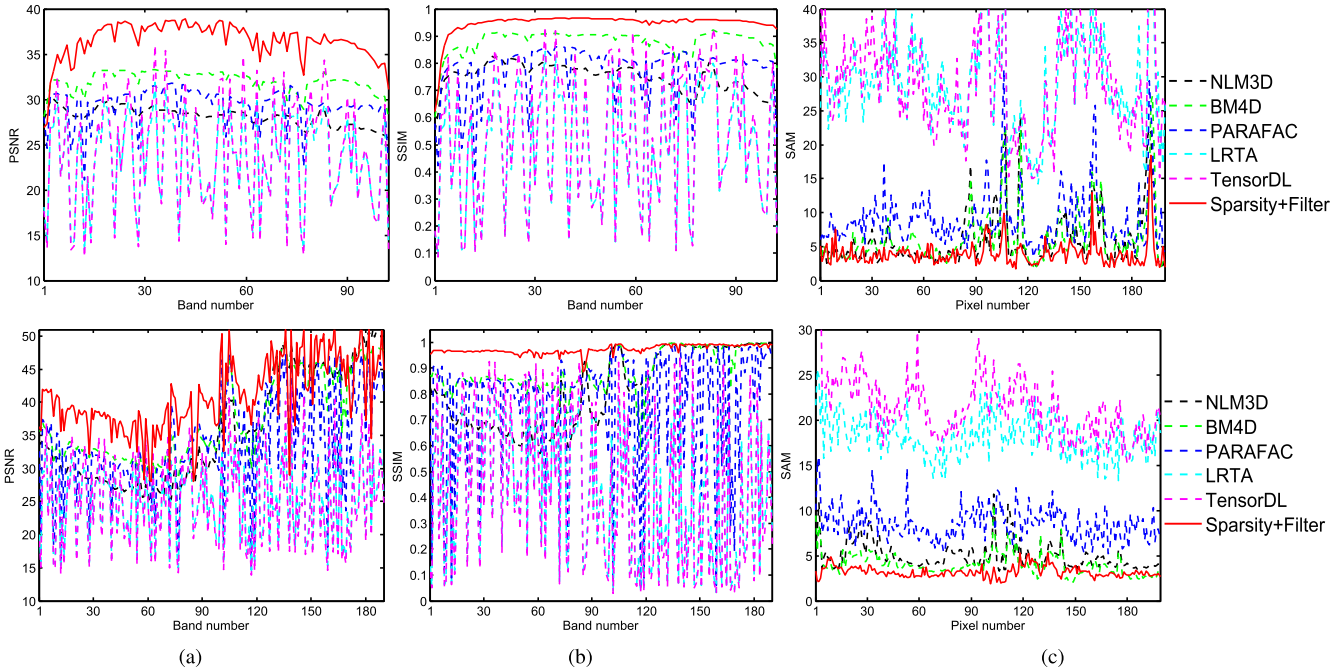

Fig. 5. PSNR and SSIM values of all denoising methods in each band of two HSIs as well as the SAM values of the first 200 pixels. (First row) Results on PaviaU. (Second row) Results on Wdc. (a) PSNR. (b) SSIM. (c) SAM.

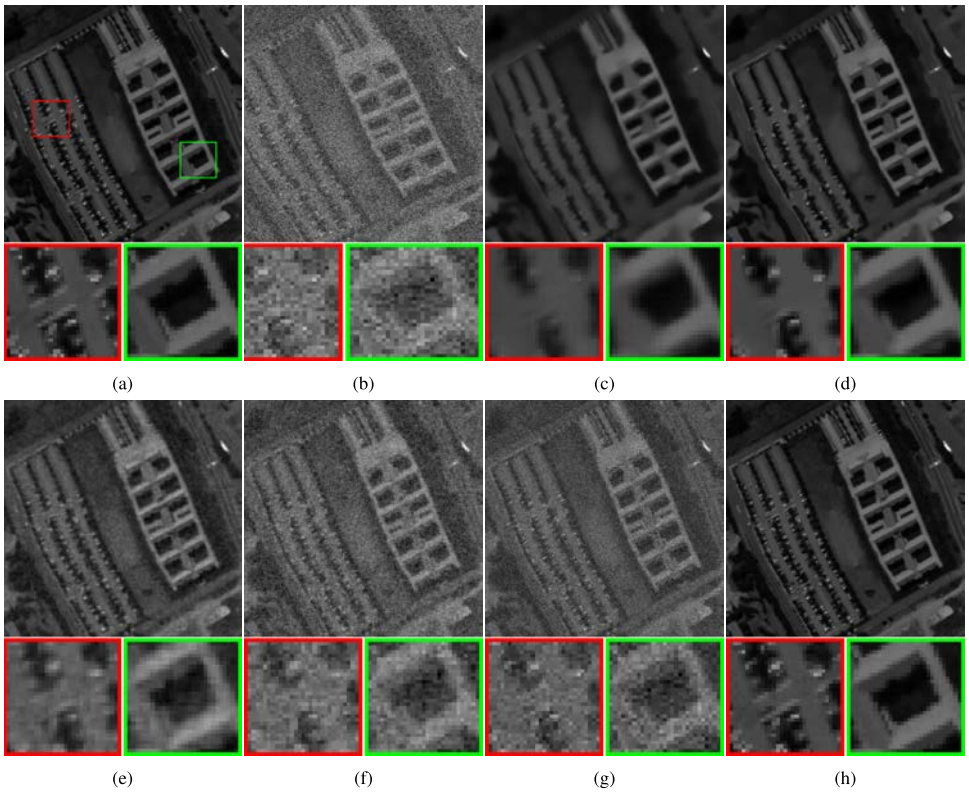

Fig. 6. Visual comparison on the denoised 58th band of PaviaU from different denoising methods. (a) Original band. (b) Noisy band. (c) NLM3D. (d) BM4D. (e) PARAFAC. (f) LRTA. (g) TensorDL. (h) Sparsity+Filter.

Since this problem is nonconvex, it is intractable to solve it directly. We turn to find a strict upper bound of the cost function in (22). According to the algebraic relation

$$|\Sigma_n + D\Sigma_y D^T| = |\Sigma_n| + |\Sigma_y| + \left|D^T \Sigma_n^{-1} D + \Sigma_y^{-1}\right| \quad (23)$$

we can further simplify (22) as

$$\min_{\Sigma_y} \|Y\|_{\Sigma_y}^2 + n_p \log|\Sigma_y| + n_p \log|D^T \Sigma_n^{-1} D + \Sigma_y^{-1}|. \quad (24)$$

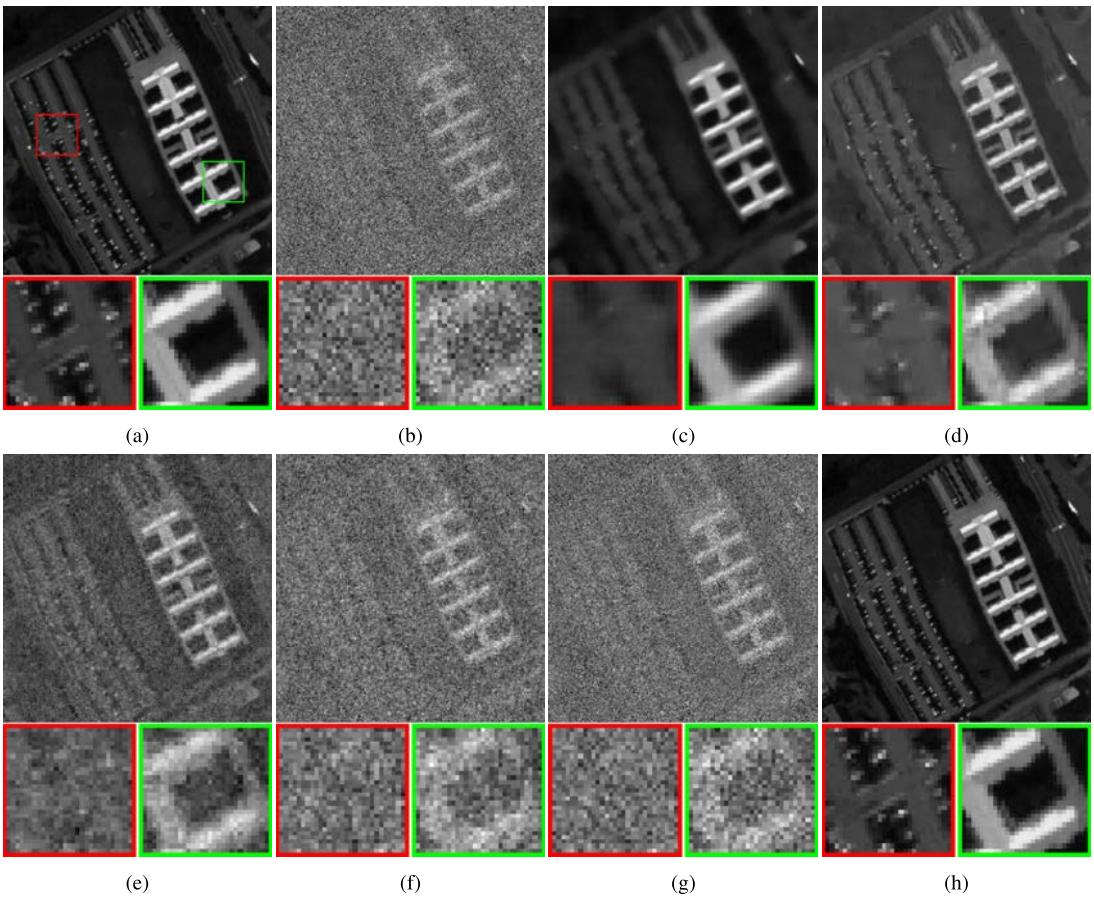

Fig. 7. Visual comparison on the denoised 13th band of PaviaU from different denoising methods. (a) Original band. (b) Noisy band. (c) NLM3D. (d) BM4D. (e) PARAFAC. (f) LRTA. (g) TensorDL. (h) Sparsity+Filter.

Letting $f(\Sigma_y^{-1}) = \log|D^T\Sigma_n^{-1}D + \Sigma_y^{-1}|$, we have the following relationship:

$$f\left(\Sigma_y^{-1}\right) = \log|D^T\Sigma_n^{-1}D + \Sigma_y^{-1}| \leq \mathbf{tr}\left(Z^T\Sigma_y^{-1}\right) - f^*(Z) \quad (25)$$

where $f^*(Z)$ is the concave conjugate function of $f(\Sigma_y^{-1})$ with an intermediate variable Z. It can be proved that the equality of the right part of (25) holds iff

$$Z = \nabla_{\Sigma_y^{-1}} f\left(\Sigma_y^{-1}\right) = \left(D^T\Sigma_n^{-1}D + \Sigma_y^{-1}\right)^{-1}. \quad (26)$$

Introducing Z and the upper bound in (25), (24) can be finally reduced to

$$\min_{\Sigma_y} \|Y\|_{\Sigma_y}^2 + n_p \log|\Sigma_y| + n_p\mathbf{tr}\left(Z^T\Sigma_y^{-1}\right) \quad (27)$$

which is a convex optimization of Σ_y and thus have a closed-form solution as

$$\Sigma_y = n_p^{-1}YY^T + Z. \quad (28)$$

C. Noise Estimation: Optimization of $\boldsymbol{\lambda}$

Given Y and Σ_y, we have the following subproblem on $\boldsymbol{\lambda}$:

$$\min_{\boldsymbol{\lambda}} \|DY - F\|_{\Sigma_n}^2 + n_p \log|\Sigma_n + D\Sigma_y D^T.|. \quad (29)$$

To optimize this nonconvex problem, we try to find a strict upper bound of the cost function in (29) similar to the graph structure learning procedure. Let $\varphi(\boldsymbol{\lambda}) = \log|\Sigma_n + D\Sigma_y D^T|$. We obtain the following relationship:

$$\varphi(\boldsymbol{\lambda}) = \log|\Sigma_n + D\Sigma_y D^T| \leq \boldsymbol{\beta}^T\boldsymbol{\lambda} - \varphi^*(\boldsymbol{\beta}) \quad (30)$$

where $\varphi^*(\boldsymbol{\beta})$ is the concave conjugate function of $\varphi(\boldsymbol{\lambda})$ with an intermediate variable $\boldsymbol{\beta}$. It can be proved that the equality of the right part of (30) holds iff

$$\boldsymbol{\beta} = \nabla_{\boldsymbol{\lambda}}\varphi(\boldsymbol{\lambda}) = \mathbf{diag}[(\Sigma_n + D\Sigma_y D^T)^{-1}]. \quad (31)$$

Given $\boldsymbol{\beta}$ and the upper bound in (30), (29) can be reduced to a convex optimization as

$$\min_{\boldsymbol{\lambda}} \|DY - F\|_{\Sigma_n}^2 + n_p\boldsymbol{\beta}^T\boldsymbol{\lambda} \quad (32)$$

which has a closed-form solution for each component λ_i as

$$\lambda_i = \sqrt{\frac{q_i}{n_p\beta_i}}. \quad (33)$$

q_i is the ith component of the vector $\boldsymbol{q} = \mathbf{diag}(QQ^T)$ with $Q = DY - F$ and β_i is the ith component of $\boldsymbol{\beta}$.

To further improve the reconstruction accuracy, a principal component analysis (PCA) dictionary D is learned from the reconstructed $\hat{X}$ after solving (18). The PCA dictionary indicates that D consists of the principle components of PCA. Specifically, considering all spectra (columns) in $\hat{X}$ as samples, PCA is conducted

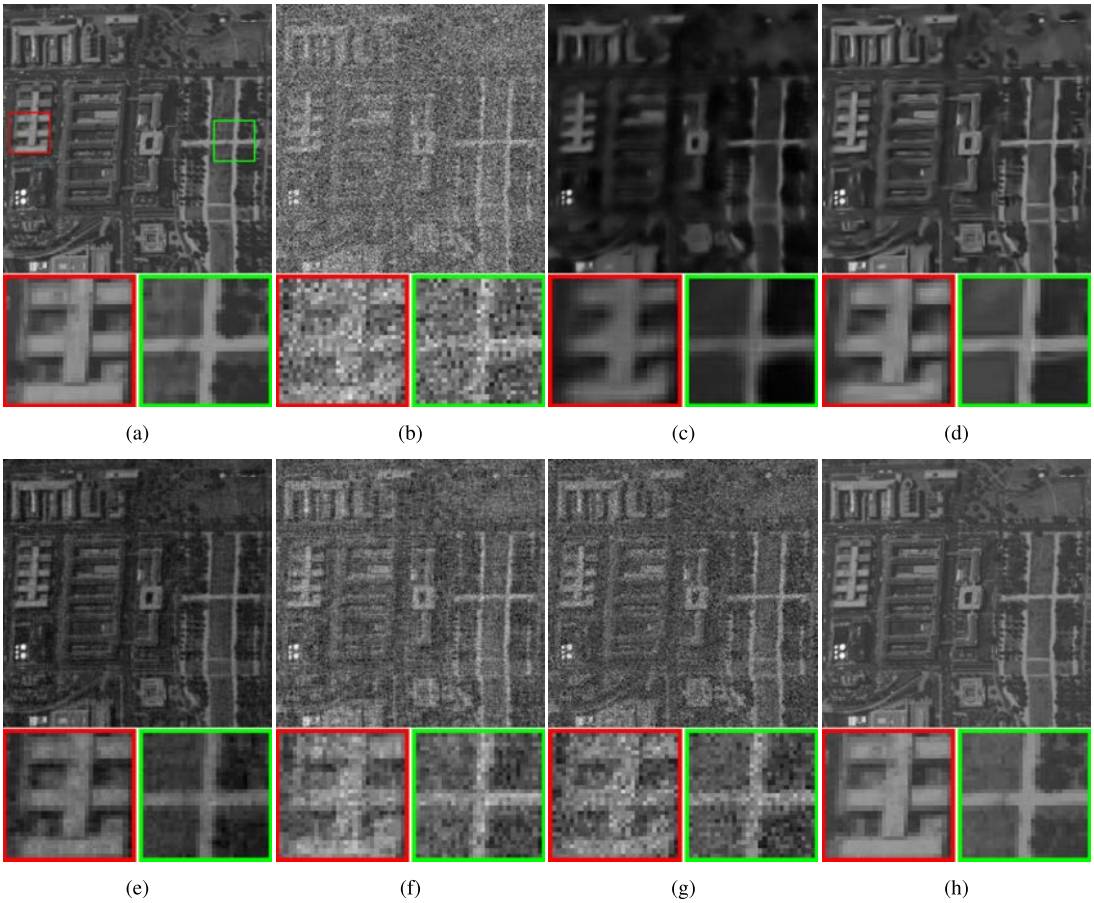

Fig. 8. Visual comparison on the denoised 50th band of Wdc from different denoising methods. (a) Original band. (b) Noisy band. (c) NLM3D. (d) BM4D. (e) PARAFAC. (f) LRTA. (g) TensorDL. (h) Sparsity+Filter.

on those samples to optimize n_b principle components $\boldsymbol{d}_i \in \mathbb{R}^{n_b}$, which form the dictionary $D = [\boldsymbol{d}_1, \ldots, \boldsymbol{d}_{n_b}]$. With such a PCA dictionary, each spectrum in the latent HSI X will be approximately sparsely represented. A similar PCA dictionary had been employed for image reconstruction in various applications [10], [37]. With the learned PCA dictionary D, (18) is solved again to refine $\hat{X}$. The dictionary learning and optimization in (18) can be conducted iteratively until convergence. Then, the intracluster filtering as (19) is employed on the reconstructed HSI $\hat{X}$ to obtain the finally denoised result. The entire denoising procedure is summarized in Algorithm 1.

Algorithm 1 Structured Sparse Coding-Based Hyperspectral Imagery Denoising With Intracluster Filtering

Input: Noisy observation F, initialized dictionary D, covariance matrix Σ_y, and noise level $\boldsymbol{\lambda}$.
while *Outer stopping criteria are not satisfied* **do**
  while *Inner stopping criteria are not satisfied* **do**
    1. Update $\Sigma_m = \Sigma_n + D\Sigma_y D^T$;
    2. Update sparse codes Y as (21);
    3. Update intermediate variable Z as (26);
    4. Learn the graph structure Σ_y as (28);
    5. Update intermediate variable $\boldsymbol{\beta}$ as (31);
    6. Estimate the noise level $\boldsymbol{\lambda}$ as (33);
  7. Reconstruct the HSI as $\hat{X} = DY$;
  8. Learn the PCA dictionary D from $\hat{X}$;
9. Divide the spectra of $\hat{X}$ into K clusters with K-means;
10. Filter the reconstructed HSI $\hat{X}$ as (19);
Output: Denoised HSI X_{rec}.

V. Experiments and Analysis

In this section, we evaluate the denoising performance of the proposed method using both simulated and real HSIs. The proposed method (denoted by 'Sparsity+Filter') is compared with five state-of-the-art HSI denoising methods, including NLM3D [15], BM4D [17], LRTA [38], PARAFAC [13], and TensorDL [8]. All of them are implemented with the codes published by the authors. Their corresponding parameters have been optimized for the best performance. For the proposed method, the spectrum dictionary D is initialized by an overcomplete discrete cosine transformation dictionary, where n_d is set as $4 * n_b$ as suggested in [39]. The noise level $\boldsymbol{\lambda}$ and covariance matrix Σ_y are initialized as a vector with all ones and an identity matrix, respectively. In Algorithm 1, the inner loop is terminated when either the maximum iteration number $N_{\max} = 300$ or the minimum update difference $\eta_{\min} = 10^{-3}$ is reached. The update difference is defined as

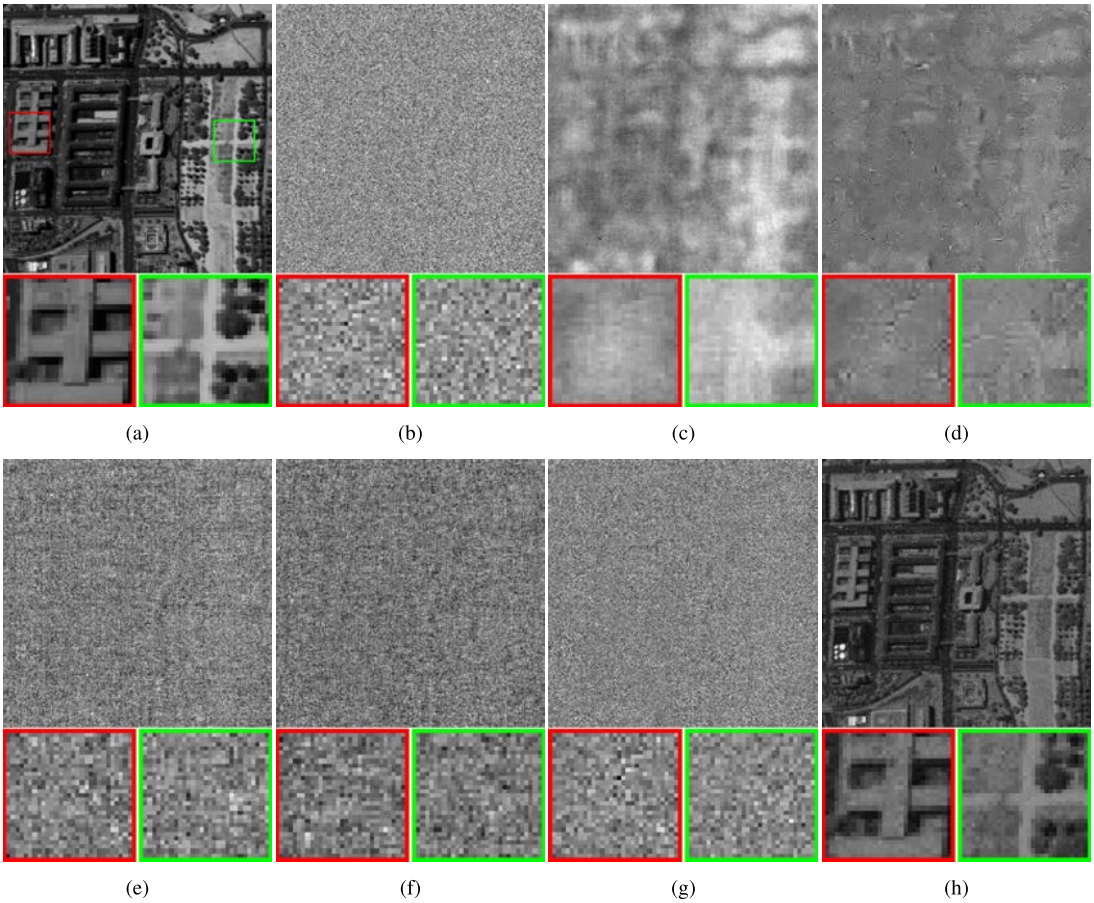

Fig. 9. Visual comparison on the denoised 120th band of Wdc from different denoising methods. (a) Original band. (b) Noisy band. (c) NLM3D. (d) BM4D. (e) PARAFAC. (f) LRTA. (g) TensorDL. (h) Sparsity+Filter.

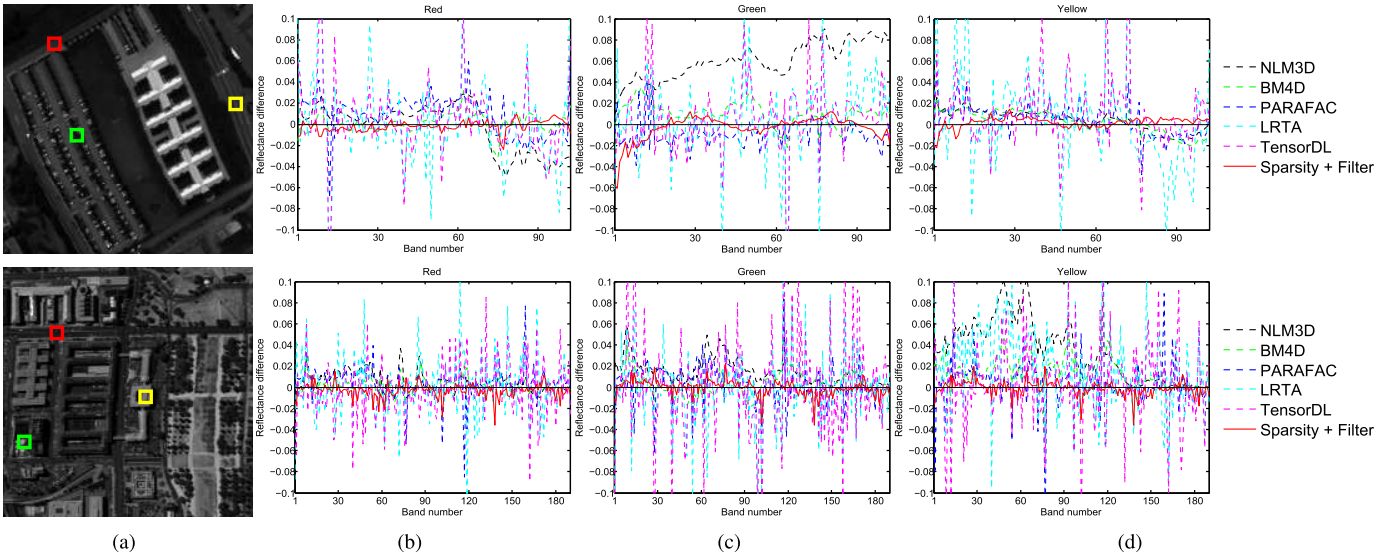

Fig. 10. Spectral reflectance difference curves of all methods on two HSIs. (a) HSI with three marked positions. (b)–(d) Curves corresponding to those three marked positions in each HSI. (First row) Curves on PaviaU. (Second row) Curves on Wdc.

$\|Y^{new} - Y\|_F / \|Y\|_F$, where Y^{new} and Y denote the updated sparse codes in the current and last iterations. In the outer loop, we run only one round of the reconstruction with the leaned PCA dictionary. The K-means++ algorithm [36] is adopted to cluster pixels in the reconstructed HSI. The cluster number $K = 30$ and the scalar $h = 0.02$ are adopted intracluster filtering. For simplicity, those settings are fixed in the following experiments.

To comprehensively assess the denoising performance of all methods, three HSI quality evaluation indexes are adopted in

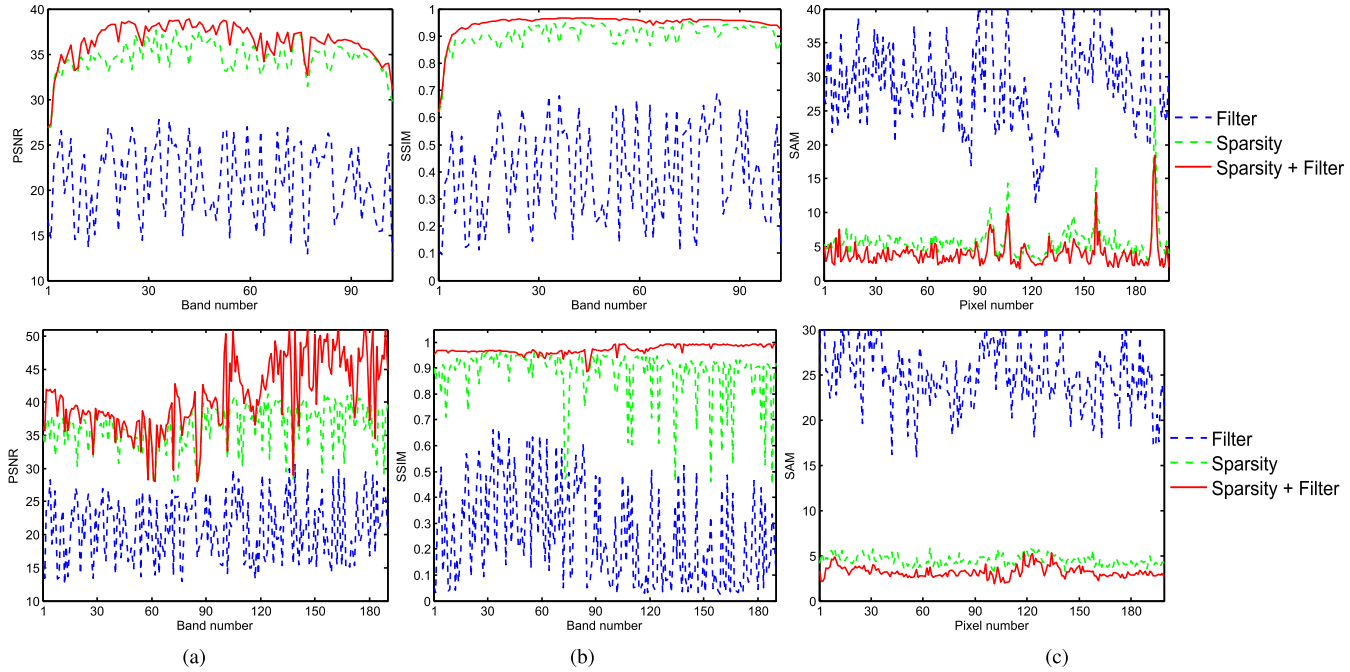

Fig. 11. PSNR and SSIM values of the proposed method and its two variants in each band of two HSIs as well as the SAM values of the first 200 pixels. (First row) The results on PaviaU. (Second row) The results on Wdc. (a) PSNR. (b) SSIM and (c) SAM.

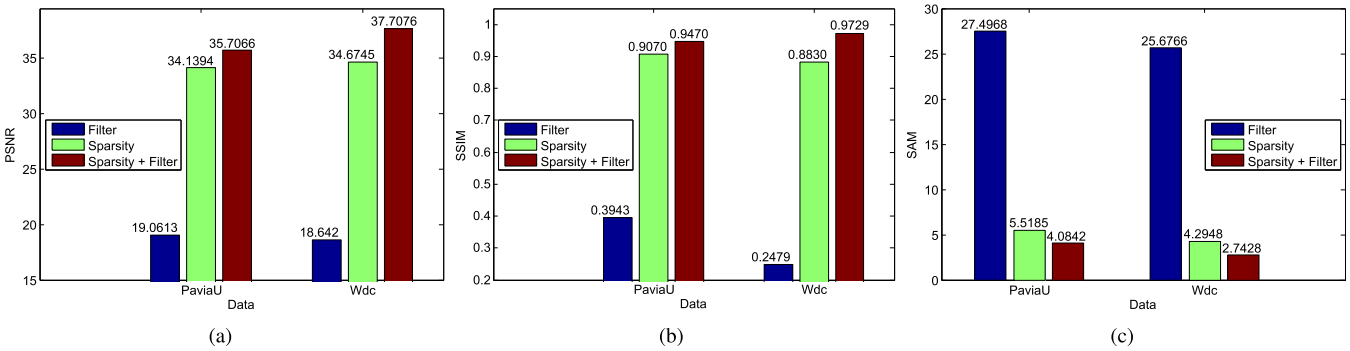

Fig. 12. Average PSNR, SSIM, and SAM bar charts of the proposed method and its two variants on two HSIs. (a) PSNR. (b) SSIM and (c) SAM.

this paper, which are the peak signal-to-noise ratio (PSNR), structure similarity (SSIM), and spectral angle mapper (SAM) [8]. PSNR and SSIM are two commonly utilized image quality indexes, which measure the similarity between two considered images based on the mean squared error and spatial structure discrepancy, respectively. Different from PSNR and SSIM, SAM is specialized in measuring the spectrum similarity of HSIs through calculating the average angle between corresponding spectrum vectors at the same position from those two considered HSIs. In the simulated denoising experiments, those three indexes are calculated for each method. Moreover, larger PSNR and SSIM and smaller SAM demonstrate better denoising performance.

A. Experiments on Simulated Noisy HSIs

In this experiment, part of ROSIS image of Pavia University and HYDICE image of Washington DC Mall are utilized as the experimental data. Their 3-D data cubes are shown in Fig. 4. For simplicity, we term those two HSIs PaviaU and Wdc. The size of PaviaU is $200 \times 200 \times 103$, while the size of Wdc is $200 \times 200 \times 191$. Each HSI X is normalized between [0, 1] before the simulation process. In the simulation process, different levels of Gaussian white noise are added across bands of X to obtain the simulated noisy HSI F, and the resulted signal-to-noise ratio of each band image is uniformly distributed in the range from 10 to 30 dB. Given the noisy HSI F, all denoising methods are conducted to reconstruct the clean X. To meet the requirements of BM4D and TensorDL, the real standard deviation of noise calculated between the ground truth X and the noisy observation F is provided as the input parameters for them.

1) Comparison With Other Competitors: For each method, Fig. 5(a) and (b) plots their curves of PSNR and SSIM values on each band of two experimental HSIs, while Fig. 5(c) gives the curves of the SAM values on the first 200 pixels. On PaviaU, the PSNR and SAM values of the proposed method (denoted by "ours") are higher than that of other

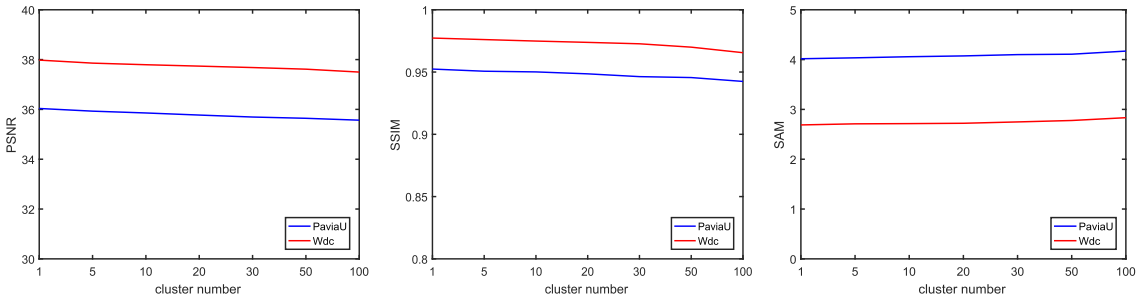

Fig. 13. Effect of cluster number on the denoising performance of the proposed method.

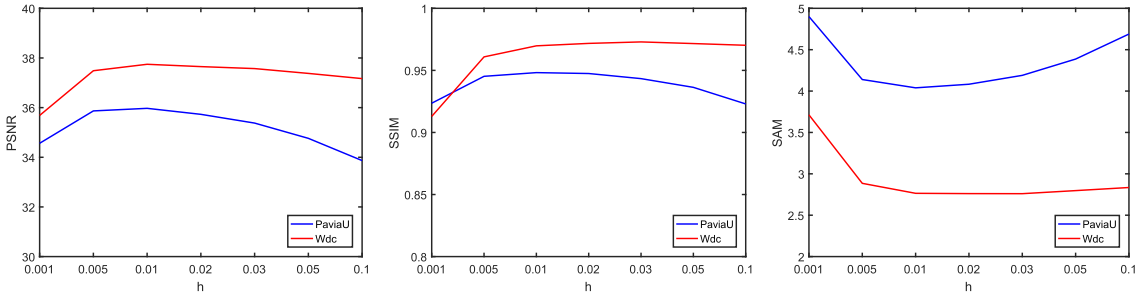

Fig. 14. Effect of parameter h on the denoising performance of the proposed method.

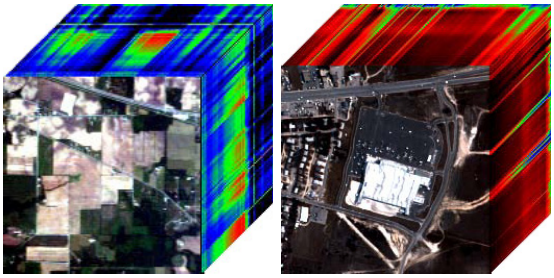

(a) (b)

Fig. 15. 3-D cubes of (a) Indiana and (b) Urban with partial bands.

TABLE I

AVERAGE PSNR, SSIM, AND SAM VALUES OF DIFFERENT METHODS ACROSS BANDS OF TWO HSIs

	Results on PaviaU			Results on Wdc		
Method	PSNR	SSIM	SAM	PSNR	SSIM	SAM
NLM3D	28.0317	0.7489	5.9968	31.0143	0.8212	4.2619
BM4D	31.8579	0.8809	5.3051	34.2876	0.8949	3.4670
PARAFAC	28.7889	0.7800	8.7460	27.9469	0.7834	9.1820
LRTA	20.1667	0.4960	25.7893	21.9832	0.4212	18.4386
TensorDL	19.8981	0.5287	26.5089	21.1854	0.4197	20.1141
Sparsity+Filter	**35.7066**	**0.9470**	**4.0842**	**37.7076**	**0.9729**	**2.7428**

competitors in most cases, while the SSIM curve of the proposed method stays above 0.9 almost in all bands, which is the highest among all methods. NLM3D, BM4D, and PARAFAC produce relatively stable curves only with small fluctuations across bands, while TensorDL and LRTA perform fluctuantly in an obvious way. On Wdc, all comparison methods perform fluctuantly in terms of SSIM and SAM, while the proposed method produces much better and more stable results. Although the proposed method also performs fluctuantly in PSNR as others, it still outperforms others in most bands. Therefore, we can conclude that the proposed method performs more stably and better than other competitors on simulated noisy HSIs. To further clarify this point, the corresponding average numerical results on PSNR, SSIM, and SAM are given in Table I. Compared with the second runner BM4D, the proposed method improves the PSNR by 3.84 dB on PaviaU and 3.42 dB on Wdc, while the corresponding SAM values decrease 1.22° on PaviaU and 0.72° on Wdc. In addition, it can be seen that the proposed method is the only one whose average SSIM values on two HSIs are larger than 0.9.

To further clarify the superiority of the proposed method in terms of denoising, we compare the denoised results of all methods visually. Figs. 6 and 7 provide the denoised 58th and 13th bands of PaviaU by all methods, where two interested areas are zoomed for details' comparison. From Figs. 6(b) and 7(b), we can find that those two selected bands are corrupted with different levels of noise. NLM3D and BM4D remove the noise corruption very well but oversmooth the spatial structures, e.g., road across the parking zone and the sharp building edges, which can be seen in the zoomed-in areas in Figs. 6(c) and (d) and 7(c) and (d). For PARAFAC, LRTA, and TensorDL, obvious noise still remains in their results. In contrast, the proposed method not only effectively removes the noise corruption but also restores the spatial structure well. Specifically, from the zoomed-in areas in Figs. 6(h) and 7(h), we can see that the road across the parking zone and the sharp building edges are well restored by the proposed method. Similarly, the proposed method also produces sharper and cleaner results for the 50th and 120th bands of Wdc than other methods, shown in Figs. 8 and 9. Especially for the 120th band in Fig. 9 where the spatial structures in the noisy band

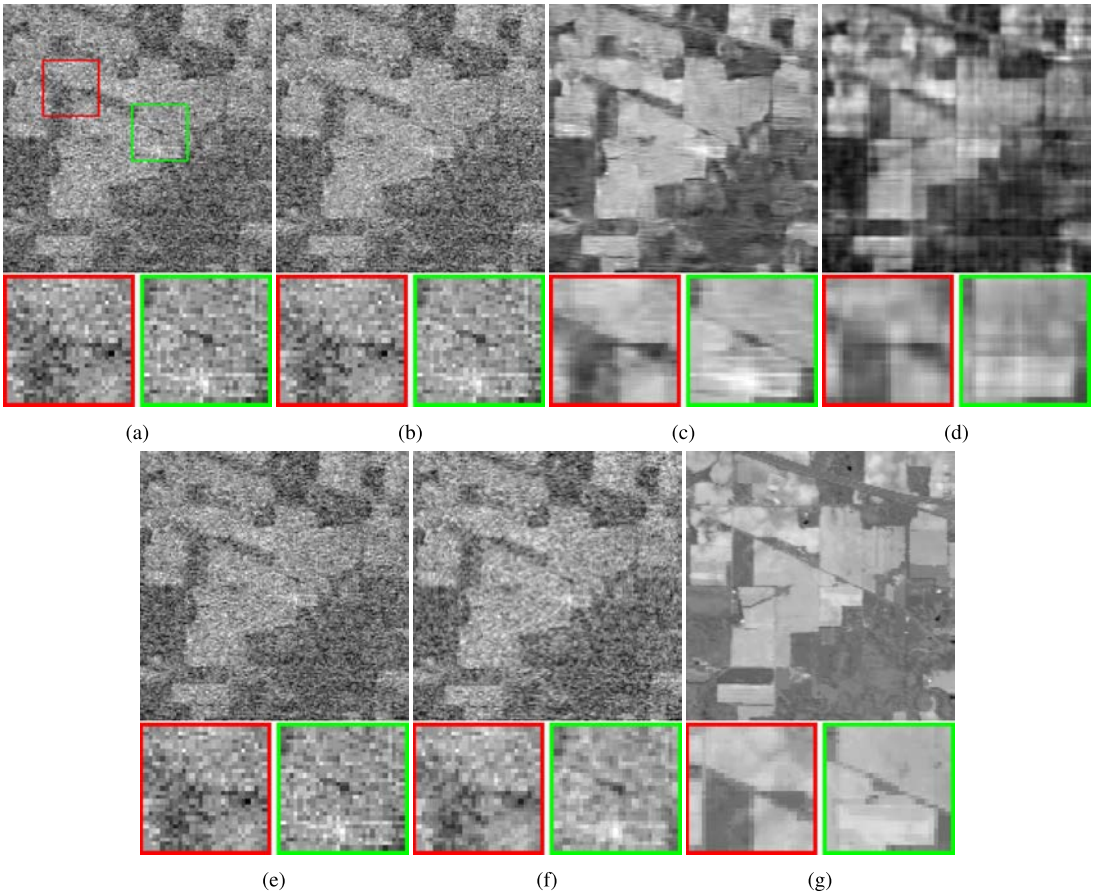

Fig. 16. Visual comparison on the denoised 109th band of Indiana from different denoising methods. (a) Original band. (b) NLM3D. (c) BM4D. (d) PARAFAC. (e) LRTA. (f) TensorDL. (g) Sparsity+Filter.

image are severely corrupted, all competitors fail to produce a relatively clean image and obvious noise remains in their denoised results. However, the proposed method still produces clean image with well-restored spatial structure shown as those zoomed-in areas in Fig. 9(h), which show the robustness of the proposed method to strong noise.

In addition, we plot the spectral reflectance difference curves for each method in Fig. 10 to illustrate the denoising performance of the proposed method on spectrum recovery [8]. The reflectance difference curve of each method is interpolated by the discrete reflectance difference between the spectrum vector from the denoised HSI and that from the ground truth at the given pixel. We select three pixels centered at the colored window for each HSI, shown in Fig. 10(a). To show a stable result, the average reflectance difference within a 3×3 neighboring area is adopted for each selected pixel. Those obtained reflectance difference curves are given in Fig. 10(b)–(d). It can be seen that the average reflectance difference of the proposed method is the closest to zero among all methods. This demonstrates that the proposed method reconstructs the spectrum more accurately than other competitors.

From the above results, we find that the proposed method performs better than others in denoising HSIs. There are two reasons. First, the proposed method unifies the structured sparse coding on spectrum domain and the intracluster filtering together, which simultaneously models the spectral correlation and spatial local and nonlocal similarity. In addition, the general noise model in (6) adapts the proposed method to various levels of noise across bands.

2) Effectiveness of the Proposed Method: The proposed method contains two crucial ingredients, namely, the structured sparse coding and the intracluster filtering. It is natural to validate whether those two parts are both crucial for good denoising performance. To this end, we compare the proposed method with its two variants on denoising the noisy PaviaU and Wdc, where the noisy HSIs are obtained in the same way as above. The first variant is termed *Sparsity*, which employs only the structured sparse coding, while the second variant termed *Filter* utilizes only the intracluster filtering for denoising. Similarly, we give the PSNR and SSIM curves of those three methods across bands of two HSIs in Fig. 11. We can find that *Sparsity* and the proposed method perform much better than *Filter*, while the proposed method stably outperforms *Sparsity* across bands of two HSIs. To further illustrate this point, the bar charts of the average numerical results of those three methods are given in Fig. 12 where we can obtain a similar conclusion. Specifically, *Filter* with intraclustering filtering alone produces the poorest results among those three methods, e.g., the obtained PSNR values on both PaviaU and Wdc are smaller than 20 dB. This is because the basic clustering procedure in intraclustering filtering is often

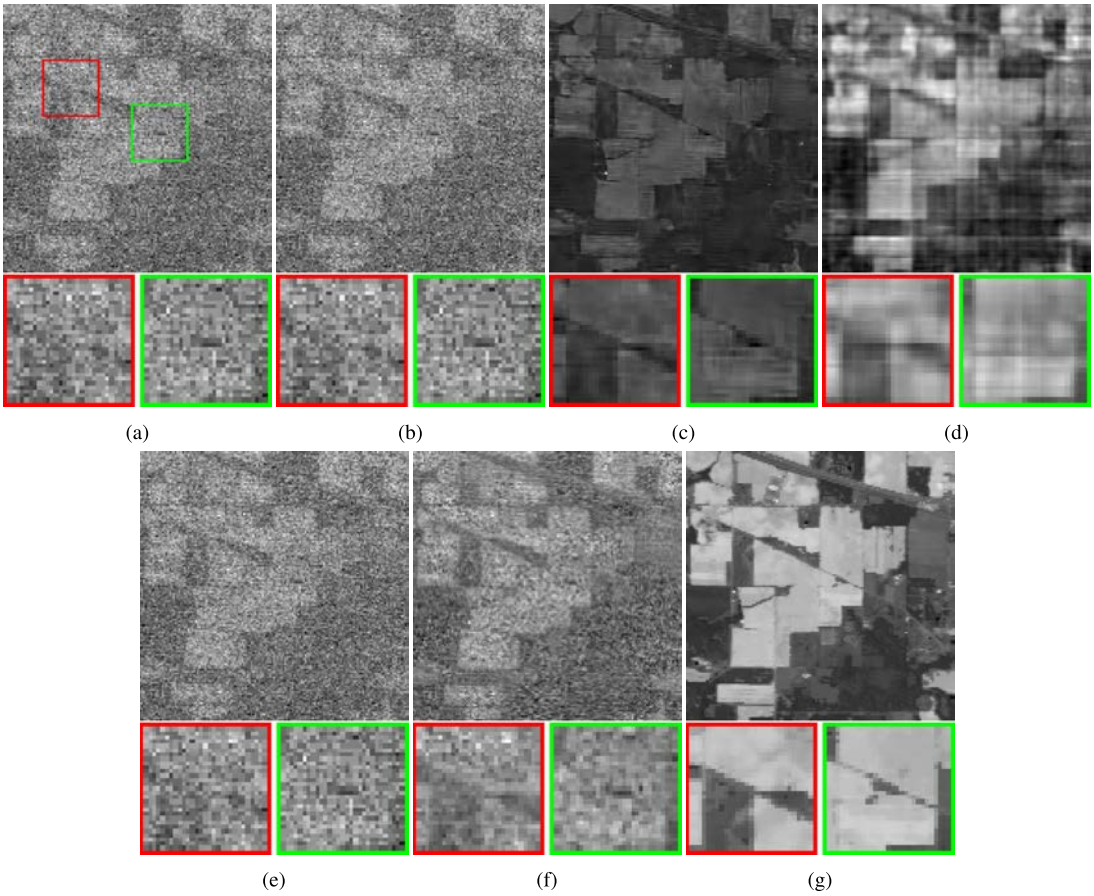

Fig. 17. Visual comparison on the denoised 219th band of Indiana from different denoising methods. (a) Original band. (b) NLM3D. (c) BM4D. (d) PARAFAC. (e) LRTA. (f) TensorDL. (g) Sparsity+Filter.

misled by the noisy spectra. Thus, its denoising performance is restricted accordingly. Although *Sparsity* with structured sparse coding alone can well reconstruct the spectrum and gives much better results than that of *Filter*, e.g., compared with *Filter*, *Sparsity* improves the PSNR by 15 dB on PaviaU and 16 dB on Wdc, the inconsistent recovery of the sparse codes caused by modeling them independently often corrupts the intracluster spectral similarity, which limits its denoising performance, e.g., the PSNR of *Sparsity* on Wdc is smaller than the proposed method by 3 dB. When fusing the structured sparse coding and intraclustering filtering, the proposed method gives the best results among all three methods. This is because the spectra reconstructed by the structured sparse coding help to improve the clustering accuracy for a better filtering and, in turn, the filtering is able to restore the intracluster spectral similarity corrupted by the structured sparse coding. Therefore, we can conclude that both the structured sparse coding and the intracluster filtering steps are crucial to denoising.

3) Effect of Parameters: In the proposed method, we have two tunable parameters, including the cluster number and the parameter h in filtering step. To analyze the effect of cluster number and parameter h on the denoising performance of the proposed method, we vary each parameter with another one fixed to conduct denoising experiments on PaviaU and Wdc data sets with the same setting as previous experiments.

First, we test the performance of the proposed method with different cluster numbers, e.g., 1, 5, 10, 20, 30, 50, and 100, and the parameter h is fixed at 0.02. The resulted PSNR, SSIM, and SAM are shown in Fig. 13. We can find that the performance is roughly insensitive to the cluster number and slightly decreases with the increasing cluster number. The reason is intuitive. According to 19, filtering results mainly depend on the top-k (e.g., $k <= 10$) similar pixels to the considered one. When cluster number varies from 1 to 100, those top-k pixels often can be collected into the same cluster as the considered one. Thus, the denoising performance can be roughly preserved. However, when the cluster number increases, pixels that are slightly similar to the considered one may be collected into different clusters and their contributions to the filtering results are eliminated. Thus, the denoising performance slightly decreases. In an extreme case where the cluster number reaches the total number of pixels in an HSI, namely, each pixel is collected into an individual cluster, the filtering step is infeasible and the proposed method degenerates to its variant "Sparsity." While the performance of the proposed method is roughly insensitive to the cluster number, the computational cost is obviously different. When the cluster number is reduced, the amount of pixels in each cluster will increase, and the filtering step will cost more on computing the weights in 19, especially when the cluster number is 1. To balance the computational cost and the performance, we fix the cluster

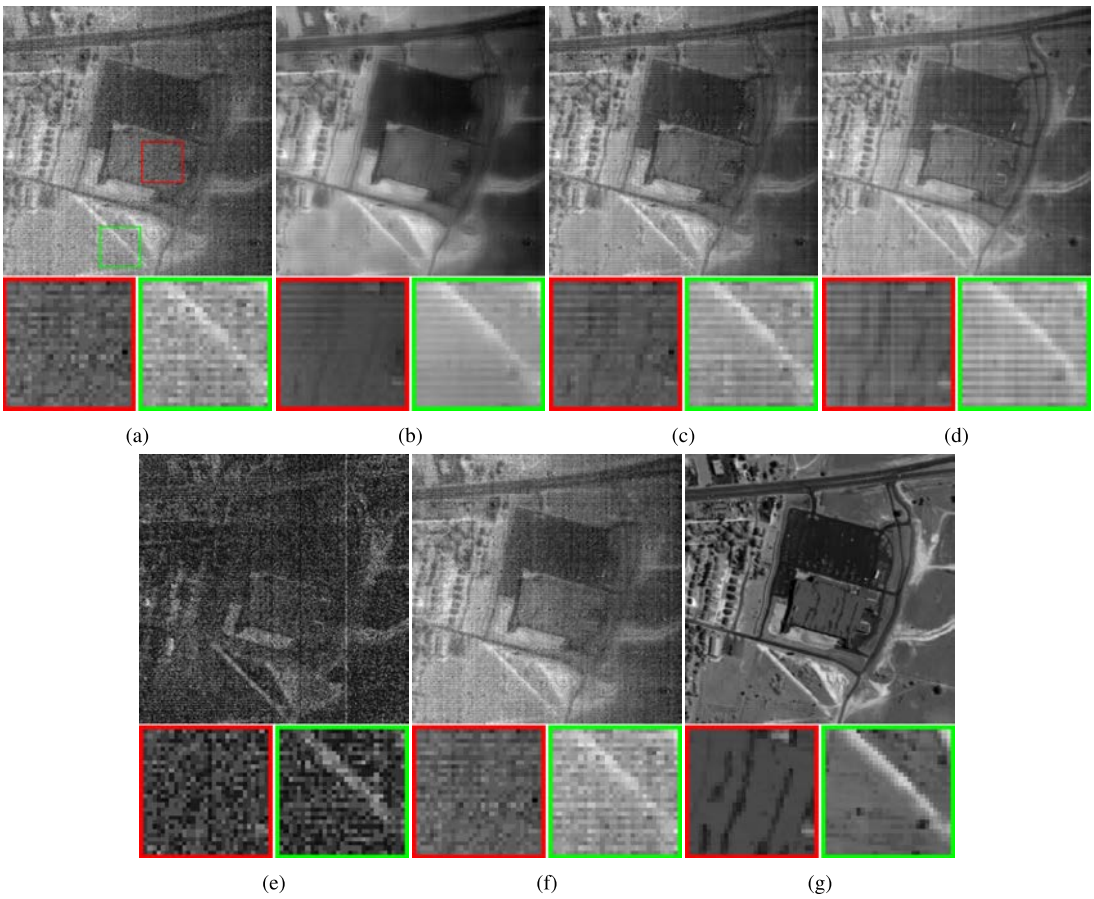

Fig. 18. Visual comparison on the denoised 104th band of Urban from different denoising methods. (a) Original band. (b) NLM3D. (c) BM4D. (d) PARAFAC. (e) LRTA. (f) TensorDL. (g) Sparsity+Filter.

number at 30 in all experiments. In addition, the adopted K-means++ algorithm [36] is able to automatically determine the initialized cluster centers for K-means based on the data distribution. Therefore, the proposed method is insensitive to the initialization of the K-means.

Second, we conduct similar experiments with varying parameter hs (e.g., 0.001, 0.005, 0.01, 0.02, 0.03, 0.05, and 0.1) in the filtering step. The cluster number is fixed at 30. We provide the corresponding results in Fig. 14. It can be seen that there exists an optimal h^* for each evaluation index. When $h > h^*$ or $h < h^*$, the performance decreases. To give the best average performance in three evaluation indices, we set $h = 0.02$ for all experiments in the main manuscript.

For simplicity, the cluster number and h are fixed for all data sets. Of course, better results can be obtained by choosing the best parameters for each data set.

B. Experiments on Real HSIs

In this section, two real HSIs are utilized to test the proposed method, which are a HYDICE Urban image and the well-known AVIRIS Indian Pines image. Hereinafter, we refer to them as Urban and Indiana for simplicity. In the following experiments, the whole image of Indiana of size $145 \times 145 \times 220$ and part of Urban of size $200 \times 200 \times 210$ are employed as the experimental data. Their 3-D data cubes are shown in Fig. 15. It has been shown that both HSIs contain some noisy bands, e.g., bands $1 - 4$, bands $103 - 112$, and bands 217–220, in Indiana [40]. More importantly, the noise levels are various across bands and the noise may be beyond Gaussian-like distribution. For example, the 109th and 219th bands in Indiana are obviously corrupted with different levels of Gaussian-like noise shown in Figs. 16(a) and 17(a), while the 104th and 207th bands in Urban are affected by two different levels of non-Gaussian noise (e.g., stripe noise) shown in Figs. 18(a) and 19(a). In the denoising process, those two noisy HSIs are directly employed as the noisy observation F for the proposed method and other five competitors.

For the Indiana scene, the denoised results of the 109th and 219th bands from all methods are visually compared in Figs. 16 and 17, where two areas of interest are zoomed for a detailed comparison. We can observe that the 109th and 219th bands are corrupted by different levels of Gaussian-like random noise. NLM3D, LRTA, and TensorDL fail to remove the noise corruption. Although BM4D and PARAFAC remove the noise corruption to some extent, they both oversmooth the sharp edges. Moreover, BM4D produces some artifacts, e.g., the undesired stripes seen as the zoomed-in areas in Figs. 16(c) and 17(c), while PARAFAC exhibits the blocking effect shown as the zoomed-in areas in Figs. 16(d) and 17(d). Compared with those competitors, the proposed method properly removes the noise corruption and well restores the sharp edges, shown as the zoomed-in areas in Figs. 16(g) and 17(g).

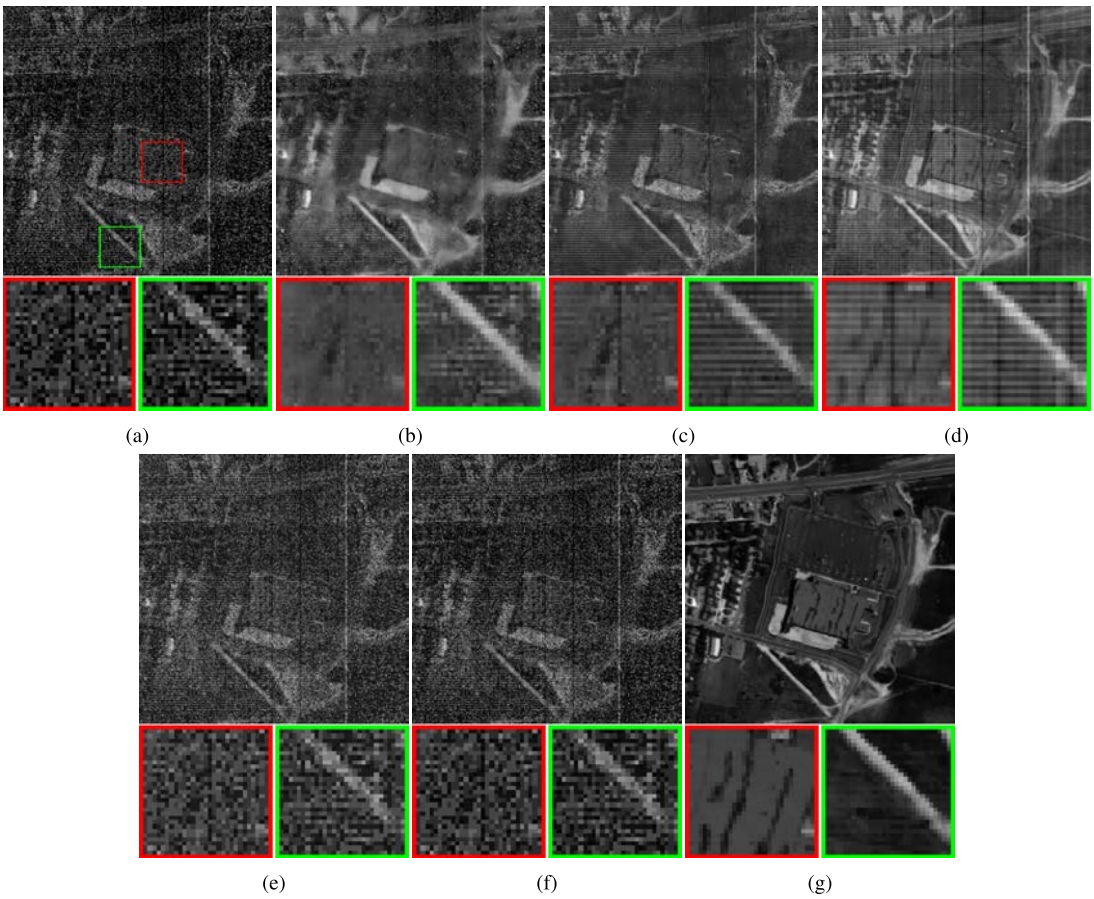

Fig. 19. Visual comparison on the denoised 207th band of Urban from different denoising methods. (a) Original band. (b) NLM3D. (c) BM4D. (d) PARAFAC. (e) LRTA. (f) TensorDL. (g) Sparsity+Filter.

For the Urban scene, we observe that the original noisy bands contain at least two different types of noises. One is Gaussian-like noise and the other is the non-Gaussian stripe noise in Figs. 18(a) and 19(a). From Figs. 18(b)–(d) and 19(b)–(d), we can find that NLM3D, BM4D, and PARAFAC perform well in removing the Gaussian-like noise, but fail on the stripe noise. While LRTA and TensorDL fail in removing both two kinds of noises shown in Figs. 18(e) and (f) and 19(e) and (f), the proposed method well removes both the Gaussian-like noise and stripe noise. In addition, the sharp edges are properly preserved with the proposed method, shown as the zoomed-in areas in Figs. 18(g) and 19(g). Although the structured sparse coding is derived based on the Gaussian noise assumption, the intracluster filtering procedure can exploit the spatial similarity to remove the non-Gaussian noise. According to the results obtained for the two considered HSIs, we can conclude that the proposed method is effective in denoising real HSIs.

VI. Conclusion

In this paper, we present a new denosing method for HSIs that combines structured sparse coding and intracluster filtering. By representing the image as a group of sparse codes on a given spectrum dictionary, we model all sparse codes together, which casts the structured sparse coding into a covariance matrix estimation problem. Then, a latent variable-based Bayesian framework is utilized to robustly capture the data-dependent structured sparsity within each spectrum under unknown noise, where the covariance matrix, sparse codes, and noise level can be jointly learned from the noisy observations. To restore the corrupted spectrum similarity in each spatial homogeneous cluster within the HSI, we further employ an intracluster filtering scheme on the reconstructed image from the structured sparse coding. Our experiments using both simulated and real images reveal that the proposed method is comparable or better than several state-of-the art denoising methods in the literature.

References

[1] D. Manolakis, E. Truslow, M. Pieper, T. Cooley, and M. Brueggeman, "Detection algorithms in hyperspectral imaging systems: An overview of practical algorithms," *IEEE Signal Process. Mag.*, vol. 31, no. 1, pp. 24–33, Jan. 2014.

[2] C.-I. Chang, "Hyperspectral target detection," in *Real-Time Progressive Hyperspectral Image Processing*. New York, NY, USA: Springer, 2016, pp. 131–172.

[3] Y. Xu, Z. Wu, J. Li, A. Plaza, and Z. Wei, "Anomaly detection in hyperspectral images based on low-rank and sparse representation," *IEEE Trans. Geosci. Remote Sens.*, vol. 54, no. 4, pp. 1990–2000, Apr. 2016.

[4] Z. Wang, N. M. Nasrabadi, and T. S. Huang, "Semisupervised hyperspectral classification using task-driven dictionary learning with laplacian regularization," *IEEE Trans. Geosci. Remote Sens.*, vol. 53, no. 3, pp. 1161–1173, Mar. 2015.

[5] X. Guo, X. Huang, L. Zhang, L. Zhang, A. Plaza, and J. A. Benediktsson, "Support tensor machines for classification of hyperspectral remote sensing imagery," *IEEE Trans. Geosci. Remote Sens.*, vol. 54, no. 6, pp. 3248–3264, Jun. 2016.

[6] H. Van Nguyen, A. Banerjee, and R. Chellappa, "Tracking via object reflectance using a hyperspectral video camera," in *Proc. IEEE Comput. Soc. Conf. Comput. Vis. Pattern Recognit. Workshops (CVPRW)*, Jun. 2010, pp. 44–51.

[7] J. P. Kerekes and J. E. Baum, "Full-spectrum spectral imaging system analytical model," *IEEE Trans. Geosci. Remote Sens.*, vol. 43, no. 3, pp. 571–580, Mar. 2005.

[8] Y. Peng, D. Meng, Z. Xu, C. Gao, Y. Yang, and B. Zhang, "Decomposable nonlocal tensor dictionary learning for multispectral image denoising," in *Proc. IEEE Conf. Comput. Vis. Pattern Recognit. (CVPR)*, Jun. 2014, pp. 2949–2956.

[9] Q. Yuan, L. Zhang, and H. Shen, "Hyperspectral image denoising employing a spectral–spatial adaptive total variation model," *IEEE Trans. Geosci. Remote Sens.*, vol. 50, no. 10, pp. 3660–3677, Oct. 2012.

[10] L. Zhang, W. Wei, Y. Zhang, C. Shen, A. van den Hengel, and Q. Shi, "Cluster sparsity field for hyperspectral imagery denoising," in *Proc. Eur. Conf. Comput. Vis.*, 2016, pp. 631–647.

[11] J. Liu, Z. Wu, J. Li, A. Plaza, and Y. Yuan, "Probabilistic-kernel collaborative representation for spatial–spectral hyperspectral image classification," *IEEE Trans. Geosci. Remote Sens.*, vol. 54, no. 4, pp. 2371–2384, Apr. 2016.

[12] N. Renard, S. Bourennane, and J. Blanc-Talon, "Denoising and dimensionality reduction using multilinear tools for hyperspectral images," *IEEE Geosci. Remote Sens. Lett.*, vol. 5, no. 2, pp. 138–142, Apr. 2008.

[13] X. Liu, S. Bourennane, and C. Fossati, "Denoising of hyperspectral images using the PARAFAC model and statistical performance analysis," *IEEE Trans. Geosci. Remote Sens.*, vol. 50, no. 10, pp. 3717–3724, Oct. 2012.

[14] A. Buades, B. Coll, and J.-M. Morel, "A non-local algorithm for image denoising," in *Proc. IEEE Comput. Soc. Conf. Comput. Vis. Pattern Recognit.*, vol. 2. San Diego, CA, USA, Jun. 2005, pp. 60–65.

[15] Y. Qian, Y. Shen, M. Ye, and Q. Wang, "3-D nonlocal means filter with noise estimation for hyperspectral imagery denoising," in *Proc. IEEE Int. Geosci. Remote Sens. Symp. (IGARSS)*, Jul. 2012, pp. 1345–1348.

[16] K. Dabov, A. Foi, V. Katkovnik, and K. Egiazarian, "Image denoising by sparse 3-D transform-domain collaborative filtering," *IEEE Trans. Image Process.*, vol. 16, no. 8, pp. 2080–2095, Aug. 2007.

[17] M. Maggioni, V. Katkovnik, K. Egiazarian, and A. Foi, "Nonlocal Transform-Domain Filter for Volumetric Data Denoising and Reconstruction," *IEEE Trans. Image Process.*, vol. 22, no. 1, pp. 119–133, Jan. 2013.

[18] B. Rasti, J. R. Sveinsson, M. O. Ulfarsson, and J. A. Benediktsson, "Hyperspectral image denoising using a new linear model and sparse regularization," in *Proc. IEEE Int. Geosci. Remote Sens. Symp. (IGARSS)*, 2013, pp. 457–460.

[19] L. Zhang, W. Wei, C. Tian, F. Li, and Y. Zhang, "Exploring structured sparsity by a reweighted Laplace prior for hyperspectral compressive sensing," *IEEE Trans. Image Process.*, vol. 25, no. 10, pp. 4974–4988, Oct. 2016.

[20] L. He and L. Carin, "Exploiting structure in wavelet-based Bayesian compressive sensing," *IEEE Trans. Signal Process.*, vol. 57, no. 9, pp. 3488–3497, Sep. 2009.

[21] C. Chen and J. Huang, "Compressive sensing MRI with wavelet tree sparsity," in *Proc. Adv. Neural Inf. Process. Syst.*, 2012, pp. 1115–1123.

[22] L. Yu, H. Sun, J.-P. Barbot, and G. Zheng, "Bayesian compressive sensing for cluster structured sparse signals," *Signal Process.*, vol. 92, no. 1, pp. 259–269, Jan. 2012.

[23] Z. Zhang and B. D. Rao, "Extension of SBL algorithms for the recovery of block sparse signals with intra-block correlation," *IEEE Trans. Signal Process.*, vol. 61, no. 8, pp. 2009–2015, Apr. 2013.

[24] J. Huang, T. Zhang, and D. Metaxas, "Learning with structured sparsity," *J. Mach. Learn. Res.*, vol. 12, pp. 3371–3412, Jan. 2011.

[25] L. Zhang, W. Wei, Y. Zhang, C. Shen, A. van den Hengel, and Q. Shi, "Dictionary learning for promoting structured sparsity in hyperspectral compressive sensing," *IEEE Trans. Geosci. Remote Sens.*, vol. 54, no. 12, pp. 7223–7235, Dec. 2016.

[26] L. Zhang, W. Wei, Y. Zhang, F. Li, C. Shen, and Q. Shi, "Hyperspectral compressive sensing using manifold-structured sparsity prior," in *Proc. IEEE Int. Conf. Comput. Vis.*, Dec. 2015, pp. 3550–3558.

[27] L. Zhang, W. Wei, Y. Zhang, C. Tian, and F. Li, "Reweighted Laplace prior based hyperspectral compressive sensing for unknown sparsity," in *Proc. IEEE Conf. Comput. Vis. Pattern Recognit.*, Jun. 2015, pp. 2274–2281.

[28] Y.-Q. Zhao and J. Yang, "Hyperspectral image denoising via sparse representation and low-rank constraint," *IEEE Trans. Geosci. Remote Sens.*, vol. 53, no. 1, pp. 296–308, Jan. 2015.

[29] S. Ji, Y. Xue, and L. Carin, "Bayesian compressive sensing," *IEEE Trans. Signal Process.*, vol. 56, no. 6, pp. 2346–2356, Jun. 2008.

[30] S. D. Babacan, R. Molina, and A. K. Katsaggelos, "Bayesian compressive sensing using Laplace priors," *IEEE Trans. Image Process.*, vol. 19, no. 1, pp. 53–63, Jan. 2010.

[31] S. Roth and M. J. Black, "Fields of experts: A framework for learning image priors," in *Proc. IEEE Comput. Soc. Conf. Comput. Vis. Pattern Recognit. (CVPR)*, vol. 2. Jun. 2005, pp. 860–867.

[32] U. Schmidt, Q. Gao, and S. Roth, "A generative perspective on MRFs in low-level vision," in *Proc. IEEE Conf. Comput. Vis. Pattern Recognit. (CVPR)*, Jun. 2010, pp. 1751–1758.

[33] D. Zoran and Y. Weiss, "From learning models of natural image patches to whole image restoration," in *Proc. IEEE Int. Conf. Comput. Vis. (ICCV)*, Nov. 2011, pp. 479–486.

[34] L. Wang, Y. Li, J. Jia, J. Sun, D. Wipf, and J. M. Rehg, "Learning sparse covariance patterns for natural scenes," in *Proc. IEEE Conf. Comput. Vis. Pattern Recognit. (CVPR)*, Jun. 2012, pp. 2767–2774.

[35] F. Chen, L. Zhang, and H. Yu, "External patch prior guided internal clustering for image denoising," in *Proc. IEEE Int. Conf. Comput. Vis.*, Dec. 2015, pp. 603–611.

[36] D. Arthur and S. Vassilvitskii, "k-means++: The advantages of careful seeding," in *Proc. 18th Annu. ACM-SIAM Symp. Discrete Algorithms*, 2007, pp. 1027–1035.

[37] W. Dong, D. Zhang, and G. Shi, "Centralized sparse representation for image restoration," in *Proc. IEEE Int. Conf. Comput. Vis. (ICCV)*, Nov. 2011, pp. 1259–1266.

[38] J. V. Manjón, P. Coupé, L. Martí-Bonmatí, D. L. Collins, and M. Robles, "Adaptive non-local means denoising of MR images with spatially varying noise levels," *J. Magn. Reson. Imag.*, vol. 31, no. 1, pp. 192–203, 2010.

[39] M. Aharon, M. Elad, and A. Bruckstein, "K-SVD: An algorithm for designing overcomplete dictionaries for sparse representation," *IEEE Trans. Signal Process.*, vol. 54, no. 11, pp. 4311–4322, Nov. 2006.

[40] L. Zhang, W. Wei, Y. Zhang, H. Yan, F. Li, and C. Tian, "Locally similar sparsity-based hyperspectral compressive sensing using unmixing," *IEEE Trans. Comput. Imag.*, vol. 2, no. 2, pp. 86–100, Jun. 2016.

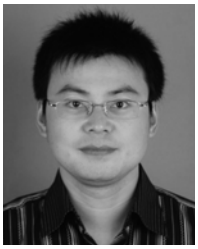

Wei Wei (M'13) received the Ph.D. degree from Northwestern Polytechnical University, Xi'an, China, in 2012.

He is currently an Associate Professor with the School of Computer Science and Engineering, Northwestern Polytechnical University. His research interests include image processing, machine learning, and pattern recognition.

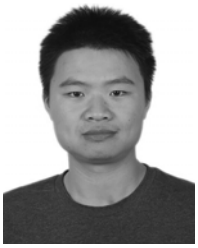

Lei Zhang (S'16) received the B.E. degree in computer science and technology from Northwestern Polytechnical University, Xi'an, China, in 2012, where he is currently pursuing the Ph.D. degree with the Shaanxi Provincial Key Laboratory of Speech and Image Information Processing, School of Computer Science and Engineering.

His research interests include hyperspectral image processing and machine learning.

Chunna Tian (M'07) received the B.S., M.S., and Ph.D. degrees from Xidian University, Xi'an, China, in 2002, 2005, and 2008, respectively.

From 2006 to 2007, she was a Visiting Student at the Visual Computing and Image Processing Laboratory, Oklahoma State University, Stillwater, OK, USA. She is currently an Associate Professor with the School of Electronic and Engineering, Xidian University. Her research interests include image processing, machine learning, and pattern recognition.

Antonio Plaza (M'05–SM'07–F'15) received the M.Sc. and Ph.D. degrees in computer engineering from the University of Extremadura, Badajoz, Spain, in 1999 and 2002, respectively.

He is currently the Head with the Hyperspectral Computing Laboratory, Department of Technology of Computers and Communications, University of Extremadura. He has authored more than 600 publications, including 197 JCR journal papers (over 140 in IEEE journals), 23 book chapters, and 285 peer-reviewed conference proceeding papers. His research interests include hyperspectral data processing and parallel computing of remote sensing data.

Prof. Plaza was a member of the Editorial Board of the IEEE GEOSCIENCE AND REMOTE SENSING NEWSLETTER (2011–2012) and the IEEE GEOSCIENCE AND REMOTE SENSING MAGAZINE (2013). He was also a member of the Steering Committee of the IEEE JOURNAL OF SELECTED TOPICS IN APPLIED EARTH OBSERVATIONS AND REMOTE SENSING (JSTARS). He was a recipient of the recognition of the Best Reviewers for the IEEE GEOSCIENCE AND REMOTE SENSING LETTERS (in 2009) and the IEEE TRANSACTIONS ON GEOSCIENCE AND REMOTE SENSING (in 2010), for which he served as an Associate Editor in 2007–2012. He was also a recipient of the Best Column Award of the IEEE SIGNAL PROCESSING MAGAZINE in 2015, the 2013 Best Paper Award of the JSTARS Journal, the most highly cited paper (2005–2010) in the *Journal of Parallel and Distributed Computing*, and the Best Paper Awards at the IEEE International Conference on Space Technology and the IEEE Symposium on Signal Processing and Information Technology. He was a Guest Editor of 10 special issues on hyperspectral remote sensing for different journals. He is an Associate Editor of the IEEE ACCESS. He served as the Director of Education Activities for the IEEE Geoscience and Remote Sensing Society (GRSS) from 2011 to 2012 and the President of the Spanish Chapter of the IEEE GRSS in 2012–2016. He was a reviewer for more than 500 manuscripts for over 50 different journals. He is currently serving as the Editor-in-Chief of the IEEE TRANSACTIONS ON GEOSCIENCE AND REMOTE SENSING.

Yanning Zhang (SM'12) received the B.S. degree from the Dalian University of Technology, Dalian, China, in 1988, the M.S. degree from the School of Electronic Engineering, Northwestern Polytechnical University, Xi'an, China, in 1993, and the Ph.D. degree from the School of Marine Engineering, Northwestern Polytechnical University, Xian, China, in 1996.

She is currently a Professor with the School of Computer Science, Northwestern Polytechnical University. Her research interests include computer vision and pattern recognition, image and video processing, and intelligent information processing.

Dr. Zhang was the Organization Chair of the Asian Conference on Computer Vision 2009 and served as the Program Committee Chair of several international conferences.